

What planetary nebulae tell us about helium and the CNO elements in Galactic bulge stars

J. F. Buell^{1*}

¹100 College Drive, SUNY College of Technology at Alfred, Alfred, NY 14843, USA

28 March 2022

ABSTRACT

Thermally pulsing asymptotic giant branch (TP-AGB) models of bulge stars are calculated using a synthetic model. The goal is to infer typical progenitor masses and compositions by reproducing the typical chemical composition and central star masses of planetary nebulae (PNe) in the Galactic bulge. The AGB tip luminosity and the observation that the observed lack of bright carbon stars in the bulge are matched by the models.

Five sets of galactic bulge PNe were analyzed to find typical abundances and central star of planetary nebulae (CSPN) masses. These global parameters were matched by the AGB models. These sets are shown to be consistent with the most massive CSPN having the largest abundances of helium and heavy elements. The CSPN masses of the most helium rich ($\text{He}/\text{H} \gtrsim 0.130$ or $Y \gtrsim 0.34$) PNe are estimated to be between 0.58 and 0.62 M_{\odot} . The oxygen abundance in form $\log(\text{O}/\text{H}) + 12$ of these highest mass CSPN is estimated to be ≈ 8.85 .

TP-AGB models with ZAMS masses between 1.2 and 1.8 M_{\odot} with $Y_{\text{ZAMS}} \approx 0.31 - 0.33$ and $Z_{\text{ZAMS}} \approx 0.19 - 0.22$ fit the typical global parameters, mass, and abundances of the highest mass CSPN. The inferred ZAMS helium abundance of the most metal enriched stars implies $dY/dZ \sim 4$ for the Galactic bulge. These models produce no bright carbon stars in agreement with observations of the bulge. These models produce an AGB tip luminosity for the bulge in agreement with the observations. These models suggest the youngest main sequence stars in the Galactic bulge have enhanced helium abundance ($Y \approx 0.32$) on the main sequence and their ages are between 2 and 4 Gyrs.

The chemical evolution of nitrogen in the Galactic bulge inferred from the models is consistent with the cosmic evolution inferred from HII regions and unevolved stars. The inferred ZAMS N/O ratio ($\log \text{N}/\text{O} \approx -0.35$) of bulge PNe with the largest CSPN masses are shown to be above the solar ratio. The inferred ZAMS N/O ratios of the entire range of PNe metallicities is consistent with both primary and secondary production of nitrogen contributing to the chemical evolution of nitrogen in the Galactic bulge.

The inferred ZAMS value of C/O is less than 1. This indicates the mass of the PNe progenitors are low enough ($M \lesssim 1.8 M_{\odot}$) to not produce carbon stars via the third dredge-up.

Key words: stars:AGB and post-AGB - abundances - mass-loss – planetary nebulae: general – Galaxy:bulge – ISM:abundances

1 INTRODUCTION

Galactic bulge planetary nebulae (GB-PNe) are an important set of stars for the study of the stellar and chemical evolution of stars. These important stars give information about the ages of different populations of stars. The central

star planetary nebulae (CSPN) mass should be related to the zero-age main sequence (ZAMS) mass of the progenitors. PNe allow direct measurements of the abundances of important atoms which are difficult to directly measure in other stars such as helium, neon and argon.

An important unsettled question about the bulge is whether it contains both old and young populations of stars or just old populations? There are two contradictory

* E-mail: buelljf@alfredstate.edu

lines of evidence about this question. Photometric studies of the luminosity of the galactic bulge main sequence turn-off (MSTO) indicate it is faint (Kuijken & Rich 2002; Zoccali et al. 2003; Brown et al. 2010; Clarkson et al. 2011). This suggests most star formation in the bulge ended around ~ 10 Gyr ago. This view has been challenged by the work of Bensby et al. (2010, 2011) using spectroscopy of stars during microlensing events. They found the position of Galactic bulge stars on the $\log g - \log T_{eff}$ plane near the MSTO and on the subgiant branch. In the same study the abundances of several elements were measured allowing a determination of chemistry. This is important since the positions of isochrones vary by $[\text{Fe}/\text{H}]$ and $[\alpha/\text{Fe}]$. To fit these stars with the correct metallicity isochrones, much younger isochrones than those used in the photometric studies were needed for a proper fit. The youngest Galactic bulge stars in Bensby et al. (2011) have inferred ages of ~ 3.0 Gyr. This suggests, in contradiction of the photometry studies, there exists a significant population of younger stars in the bulge.

Nataf and Gould (2012) suggested a way to reconcile these two disparate interpretations. They suggested that there is a population which is older than that suggested by Bensby et al. (2010, 2011) but younger than 10 Gyr suggested by photometric studies. They argue such a population reconciles these two disparate observations with essentially two old populations; one with enhanced values of Y and one with normal values of Y . They argue that both the photometric and spectroscopic studies use of non-helium enhanced isochrones give the wrong inferred ages and masses of bulge stars. Their argument is that if helium enhanced isochrones are used for comparison to the MSTO in the photometric studies, a younger age would be indicated. If helium enhanced isochrones are used to compare to the results from the spectroscopic studies of (Bensby et al. 2010, 2011) older ages would be indicated. This would bring these contradictory results at least nearer to agreement.

Nataf et al. (2011) also found indirect evidence that there are stars with enhanced Y in the bulge. They attributed the anomalous Galactic bulge red giant branch bump to a population of stars with an enhanced value of Y ($Y \sim 0.35$).

An enhanced value of Y in ZAMS stars is not unprecedented. Globular clusters in the Milky Way and the Magellanic Clouds show evidence of the existence of multiple populations with distinct values of Y . The extensive spectroscopic evidence is reviewed in Gratton, Carretta and Bragaglia (2011) and the photometric evidence of multiple main-sequences, sub-giant branches, red giant branches and horizontal branches in the same globular cluster is reviewed in Piotto (2009). In many (and possibly all) globular clusters there are at least two chemically distinct populations. The older population (primary) consists of stars with scaled-solar abundances and a helium abundance which can be determined by linearly interpolating in Z from the primordial helium abundance, Y_0 , to the solar helium abundance, Y_\odot . The slightly younger population (secondary) consists of stars with an enhanced abundance of helium (ΔY) which can be very modest (≈ 0.01) or large (≈ 0.12). The enhancement of helium is defined as the increase of the helium fraction over what would be determined from the equation:

$$Y = Y_0 + (dY/dZ)Z \quad (1)$$

where Z is the metallicity.

There are several available abundance studies of Galactic bulge PNe (hereinafter GB-PNe) which measure the abundance of helium (Ratag et al. 1992, 1997; Cuisinier et al. 2000; Liu et al. 2001; Escudero, Costa & Maciel 2004; Exeter, Barlow & Walton 2004; Wang and Liu 2007; Chiappini et al. 2009). All of these studies show some GB-PNe have an elevated He/H (Defined here as $\text{He}/\text{H} > 0.120$). In each of these studies the highest level of He/H for each lies between 0.135 and 0.22. For a PN in the disc or other region where there is active star formation an elevated He/H would be interpreted as the result of helium enhanced material being mixed up from the interior to the surface of the star. The amount of this enhancement is greatest for intermediate-mass stars (defined as $M \gtrsim 3.5 M_\odot$). The surface helium abundance of intermediate-mass stars is increased by the action of the second dredge-up (SDU), the third dredge-up (TDU) and the action of hot-bottom burning (HBB). HBB occurs at the base of the convective envelope of a thermally pulsing asymptotic giant branch (TP-AGB) star when the temperature at the base becomes high enough for the CN cycle to operate. HBB is limited to intermediate-mass stars ($\gtrsim 3.5 M_\odot$) and converts C to N while producing some He. The SDU occurs when the star enters the early-AGB (E-AGB) and material which experienced complete hydrogen burning is mixed up to the surface. A result of SDU is to raise the surface abundance of helium. Theoretically to get a SDU a star needs a ZAMS mass of $\gtrsim 4.0 M_\odot$ (Boothroyd and Sackmann 1999). The TDU occurs near the end of a helium shell flash when during the TP-AGB the convective envelope penetrates into a region where partial helium burning has taken place. However, to significantly enhance the abundance of helium and nitrogen requires an intermediate-mass star ($M \gtrsim 3.5 M_\odot$). The lifetime of such a star is short ($\lesssim 0.5$ Gyr).

If intermediate-mass stars are the progenitors of the high helium bulge PNe then they would come from a very young population. This hypothetical very young population would be younger than the results of Bensby et al. (2010, 2011) would indicate. Since a significant number of the bulge PNe have high helium abundances generally associated with intermediate-mass stars, but there are not significant numbers of intermediate-mass stars in the bulge, there must be an alternative explanation of the observed high helium abundances. The observed range of GB-PNe He/H is 0.09-0.20. Assuming the progenitor has near solar abundances, $Y \approx 0.27$ and $Z \approx 0.017$ (van Saders and Pinsonneault 2012), to produce a helium abundance this high requires a star of mass of $\gtrsim 4 M_\odot$ (Groenewegen & de Jong (1993); Marigo, Girardi, & Bressan (1999)) with a lifetime of $\lesssim 0.4$ Gyr. Main sequence stars of this mass are not observed in the bulge. It seems unlikely there are stars of this mass in the bulge since it would mean there would be AGB stars brighter than seen in the bulge. If intermediate-mass stars exist in the bulge, it would mean main sequence stars with masses between 2 and $4 M_\odot$ would also exist in the bulge. These 2- $4 M_\odot$ would produce bright carbon stars. This contradicts the observation that the C-stars in the bulge are faint. Faint carbon stars are interpreted as carbon-enriched low-mass stars resulting from a binary mass-transfer event.

The alternative is that the progenitors of these PNe are

older low-mass stars which formed with high helium abundance. The PNe abundances would then reflect the initial abundances with minor modifications due to the first dredge up (FDU) only. The FDU effects stars of all mass and occurs when the star enters the red giant branch (RGB). During the FDU the abundances of He and N are slightly increased at the expense of a decrease in the C abundance. Buell (2012) (hereinafter Paper I) presented a similar model to explain the two PNe in globular clusters (JaFu 1 and JaFu 2) both of which have elevated helium abundances but are clearly from an old, low-mass population. Paper I showed the global parameters of both the PNe (helium abundance, oxygen abundance, mass of central star) and the parameters inferred from the host cluster (metallicity and progenitor mass) can be matched by low-mass, helium enhanced models.

The goal of this paper is to test if the GB-PNe can be explained with a low-mass model and to use their observed global parameters to infer the ZAMS mass and the ZAMS Y value. In Section 2 the TP-AGB models are discussed. In Section 3 the abundances and CSPN masses of GB-PNe as well as other relevant observations are reviewed with the goal of determining appropriate global averages to compare to the models. In Section 4 the models are presented and compared to the observations. In Section 5 the implications are discussed. In Section 6 conclusions and suggestions for further work are presented.

2 MODELS

To model the evolutionary behavior of the stars the model described in Paper I is used. Briefly, this model calculates the structure of the envelope during the interpulse period of the TP-AGB by getting the luminosity from a core-mass luminosity relation. The effects of pre-TP-AGB evolution are modeled using fits to published models. Most of the relevant details of this model are explained in Buell et al. (1997), Buell (1997), and Gavilan, Buell, & Molla (2005). In paper I the most significant update to the model was an updated rule for treating the mass-loss during the red giant branch (RGB) and early-AGB (E-AGB) phases. This is a significant model input, especially for low-mass ZAMS stars which can lose an appreciable fraction of their mass during the RGB and E-AGB. In paper I, particular attention was paid to the effect of an enhanced helium abundances on mass-loss during these stages. The mass-loss in these stages was found by integrating the mass-loss rate formula over the Padova tracks. There is an important point to note, in paper I the calculation of pre-TP-AGB mass-loss model, as noted by the referee of that paper, the evolution of the star and the mass-loss rates are not coupled. The amount of mass-loss found with these equations are quite reasonable but the reader should be aware of it. For the masses of the stars modeled here ($M=1.1-1.8M_{\odot}$) any errors in the pre-TP-AGB mass-loss will not have a large effect on the subsequent evolution of the star.

2.1 Elemental abundances

The solar abundance set used in this paper is from Asplund, Grevesse, & Sauval (2005). This set was chosen because the oxygen abundance ($\epsilon(\text{O}) = 8.66$) is similar to

that found in Galactic HII regions such as the Orion Nebula. A typical value of oxygen for the Orion Nebula is slightly higher, e.g. $\epsilon(\text{O}) = 8.74$ (e.g. Simón-Díaz et al. 2011).

Abundances for stars are usually published as in terms of $[\text{Fe}/\text{H}]$. At sub-solar $[\text{Fe}/\text{H}]$ the α elements are known to be enhanced. At $[\text{Fe}/\text{H}] \lesssim -1.0$ the α elements are enhanced relative to iron by a constant factor. The level of the α plateau is expressed as

$$[\alpha/\text{Fe}] = k_1 \quad (2)$$

where k_1 is an adjustable parameter. In this model this parameter which will be set to approximately +0.4. At a value of $[\text{Fe}/\text{H}] \approx -1$ the value of $[\alpha/\text{Fe}]$ begins to decrease linearly and reaches a value of zero at $[\text{Fe}/\text{H}] = 0$. The position of this knee in the distribution is given by

$$[\text{Fe}/\text{H}]_{\text{knee}} = k_2. \quad (3)$$

The mass fraction of helium Y is computing an intermediate scaled solar value, Y_{ss} is computed by

$$Y_{ss} = Y_0 + \frac{dY}{dZ}Z \quad (4)$$

where Y_0 is the primordial helium mass fraction and $\frac{dY}{dZ}$ is the slope of the relationship between Y and Z . The mass fraction of helium is then enhanced by an adjustable factor ΔY . The equation is given by

$$Y = Y_{ss} + \Delta Y. \quad (5)$$

Since the element nitrogen shows considerable variation the abundance of nitrogen can be enhanced by a factor ΔN . When nitrogen is enhanced the value of Z is enhanced by the same amount. The mass fraction of hydrogen is calculated from

$$X = 1 - Y - Z. \quad (6)$$

2.2 Red giant mass-loss

The mass-loss which occurs on the red giant branch (RGB) is very important for low-mass stars, which in some extreme cases may prevent the star from even reaching the TP-AGB. Most of the pre-TP-AGB mass-loss occurs during the RGB. The standard method to determine the amount of mass-loss is to use Reimers' Law (Reimers 1975) given by

$$\dot{M} = \eta \frac{LR}{M} \quad (7)$$

where L , R and M are the stellar luminosity, radius and mass, respectively in solar units. However, in this paper the pre-TP-AGB mass-loss was calculated using an updated and modified version of the Reimers formula of (Schröder and Cuntz 2005) given by

$$\dot{M} = \eta \frac{LR}{M} \left(\frac{T_{\text{eff}}}{4000\text{K}} \right)^{3.5} \left(1 + \frac{g_{\odot}}{4300g_{\star}} \right) \quad (8)$$

where T_{eff} is the effective stellar temperature, g_{\star} is the surface gravity of the star in cgs units. Values of 27400cgs^{-2} for g_{\odot} and 8.0×10^{-14} for η were adopted, which are the values recommended by (Schröder and Cuntz 2005). This new mass-loss rule appears to give better results for horizontal branch masses than the Reimer's rate (Schröder and Cuntz 2005).

This mass-loss law was applied to the variable Y stellar evolution tracks from the Padova stellar evolutionary library (<http://pleadi.pd.astro.it>) described in detail in Bertelli et al. (2008) and Bertelli et al. (2009). To determine the red giant mass-loss the mass-loss rate was integrated from the beginning of the red giant branch (encoded in the Padova files as brgbs) up to the tip of the red giant branch (encoded as trgb) using the trapezoidal rule. The amount of mass-loss between time steps in the models is given by

$$\Delta M_i = \frac{1}{2}(\dot{m}_{i+1} + \dot{m}_i)(t_{i+1} - t_i) \quad (9)$$

where t_i and t_{i+1} are the model times and \dot{m}_{i+1} and \dot{m}_i are the mass-loss rates at the corresponding times. The total mass-loss is determined by summing all of the ΔM_i s.

Paper I gives the mass-losses for the RGB and E-AGB for the Padova models with metallicities of solar ($Z = 0.017$) and lower. Since bulge metallicities are higher (and potentially super-solar) the mass-losses for the higher than solar metallicities are presented in this paper.

The mass-losses on the RGB as a function of the ZAMS mass for all available values of Y for $Z = 0.04$ and $Z = 0.07$ are shown in Figure 1 by the points. In all panels it is evident the amount of mass-loss decreases as Y increases. This occurs because stars with higher values of Y means the RGB star will have smaller radii and higher surface gravity due to the lower opacity in the outer layers. These factors lower the mass-loss rates and the total mass-loss.

The RGB mass-loss was fit using two linear fits for higher and lower ZAMS masses. The transition point between the fits was determined by visually estimating the mass where the slope appears to change. This mass is typically found around a ZAMS mass of $0.8\text{--}0.9 M_\odot$. The higher mass fit was terminated where the high mass line crosses the horizontal axis. This termination point was estimated visually. For masses larger than $\approx 2.0 M_\odot$ the mass-loss is 0. The equations of the linear fits for low and high masses are given by $\Delta M_{\text{RGB,low}}$ and $\Delta M_{\text{RGB,high}}$. To make the fits work the fitting was done by excluding the $M \leq 0.9 M_\odot$ models. These can be safely excluded since the mass-loss for these very low-mass stars eliminates their envelope before the tip of the RGB is reached and such models will not be considered in this paper. Visual inspection indicates the fits are in good agreement to the mass-loss calculations.

The equations for $\Delta M_{\text{RGB,low}}$ and $\Delta M_{\text{RGB,high}}$ are given by

$$\Delta M_{\text{RGB,low}} = a_{11}M + a_{10} \quad (10)$$

$$\Delta M_{\text{RGB,high}} = a_{21}M + a_{20}. \quad (11)$$

The mass-loss is found by calculating the value of both ΔM s and finding the maximum value. If the mass-loss is found to be negative then the value of the mass-loss is set to 0. The coefficients of these equations for the different values of Y and Z are shown in Table 1.

A couple of caveats need to be noted. No attempt has been made yet to calibrate this mass-loss, which will be done in a later paper. However, the mass-loss values from these equations appear to be reasonable. For example a $1.0 M_\odot$ $Y = 0.26$ $Z = 0.017$ star would experience $0.28 M_\odot$ of mass-loss on the RGB which is typical of other models. A typical globular cluster turn-off mass of $0.80 M_\odot$ with $Y = 0.245$ and $Z = 0.0008$ gives a RGB mass-loss of $0.22 M_\odot$. This is

reasonable since it gives a zero-age horizontal branch mass of approximately $0.58 M_\odot$ which is similar to measured values (e.g. Gratton et al. 2010).

It should be noted, as suggested by the referee of paper I, that the method used to find the mass-loss is not consistent with the stellar evolution models. As the star loses mass its surface gravity would decrease causing the star to expand. For the models used this would result in a higher mass-loss rate near the tip of the RGB and a greater amount of mass-loss on the RGB (and the E-AGB) than is calculated here. However, this effect should be relatively small since the deviation will only be really significant at the tip of the RGB. Although the method used here is not strictly consistent the relative differences in mass-loss due to the effect of the ZAMS helium abundances and the ZAMS metallicity should be correct.

It was noted by the referee of this paper that Miglio et al. (2012) argued the RGB mass loss inferred by asteroseismology for the old, metal-rich ($Z \approx 0.04$) open cluster NGC6791 is 0.09 ± 0.03 . This is approximately one half of the red giant mass loss as determined from the formulas above. The MSTO mass of NGC6791 is $1.23 M_\odot$. The amount of RGB mass loss predicted for the prescription here is $\sim 0.17 M_\odot$. The relatively small difference between the mass loss will make little difference to the subsequent AGB evolution. In the bulge the most massive PN progenitors will have masses between 1.2 and $1.8 M_\odot$ and only a relatively small amount of mass ($\lesssim 0.1 M_\odot$) is lost on the RGB and E-AGB. Most of the mass loss occurs on the TP-AGB when the star evolves to the superwind phase. During this phase the mass loss rates are 10^{-5} to $10^{-4} M_\odot \text{yr}^{-1}$. In models when the star reaches the superwind phase with an additional $0.1 M_\odot \text{yr}^{-1}$ of envelope mass, it produces a model CSPN with an observationally negligibly different mass. To verify this some models were run with a pre-AGB mass loss with one half of the value from the prescription above and the difference in the CSPN mass is found to be small.

2.3 Mass-loss on the early-AGB

The same procedure to determine the mass-loss on the RGB was applied to the early-AGB (E-AGB) portions of the Padova tracks. An additional condition of starting the mass-loss when the temperature was below 4500K was assumed since this mass-loss law is applicable only to K and M stars.

Figure 2 shows the calculated mass-loss during the E-AGB and the fits to these mass-losses. The mass-loss on the E-AGB is fit using 4 fits in different regions of mass. The lowest mass range ($M \lesssim 1.5 M_\odot$) is fit via a cubic, the next mass range up ($1.5 M_\odot \lesssim M \lesssim 2.0 M_\odot$) is fit using a quadratic fit. The next mass range up ($2.0 M_\odot \lesssim M \lesssim 4.5 M_\odot$) is fit using a linear fit. Finally the highest masses are fit using a constant value of mass-loss. The points of intersection between adjacent fits were visually estimated. This procedure gives a good fit to the model mass-losses.

The equations for the E-AGB mass-loss in the first two mass regions are given by

$$\Delta M_{\text{E-AGB}} = a_{13}M^3 + a_{12}M^2 + a_{11}M + a_{10} \quad (12)$$

and

$$\Delta M_{\text{E-AGB}} = a_{22}M^2 + a_{21}M + a_{20} \quad (13)$$

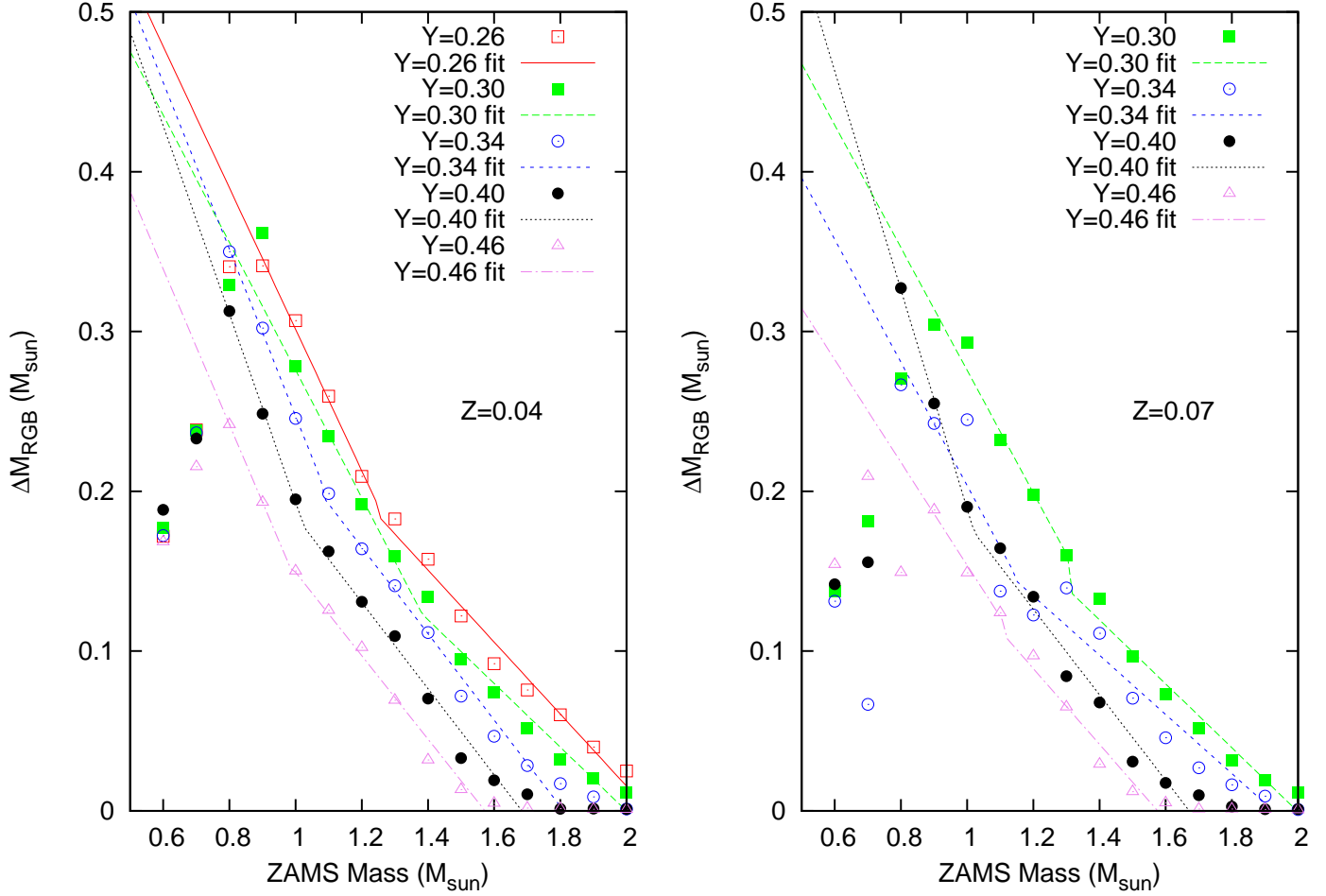


Figure 1. Each panel in the figure shows the calculated mass-loss on the red giant branch for the $Z=0.04$ and 0.07 for the available values of Y . The red open squares, green filled squares, blue open circles, black closed circles and violet triangles are the calculated mass-losses for $Y=0.26, 0.30, 0.34, 0.40$ and 0.46 , respectively. The red solid, green dashed, blue short dashed, black dotted and violet long-dashed dotted lines are the fits for the $Y=0.26, 0.30, 0.34, 0.40$, and 0.46 mass-losses, respectively.

Table 1. Red giant mass-loss coefficients

Z	Y	a_{11}	a_{10}	a_{21}	a_{20}
0.040	0.26	-0.442678	0.744023	-0.225394	0.466268
0.040	0.30	-0.638065	0.929548	-0.230933	0.455032
0.040	0.34	-0.522	0.769042	-0.270372	0.489416
0.040	0.40	-0.589165	0.782297	-0.269874	0.454302
0.040	0.46	-0.48654	0.630983	-0.26096	0.410264
0.070	0.30	-0.3836	0.659316	-0.200032	0.399528
0.070	0.34	-0.384918	0.588526	-0.185168	0.356611
0.070	0.40	-0.684775	0.873781	-0.267901	0.447723
0.070	0.46	-0.3217	0.475414	-0.23702	0.373474

where M is the mass of the star on the ZAMS. Only the coefficients of first two regions have been included in Table 2 to save space and since no models of sufficient mass which need the fits for the upper regions are calculated in this paper. The coefficients for lower metallicities are presented in paper I. The E-AGB mass-loss is calculated by finding the intersection of the two regions and then choosing the appropriate region and plugging into the corresponding equation.

2.4 Core mass at the first pulse

From the Padova stellar evolution library the core mass at the onset of the first thermal pulse as a function of the ZAMS mass was extracted. The tables with this information are found under the agb files are found at vizier.u-strasbg.fr in the catalog J/A+A/508/355. Figure 3 shows the mass of the carbon-oxygen core as a function of mass for several values of Y and Z . An important point to note is that as

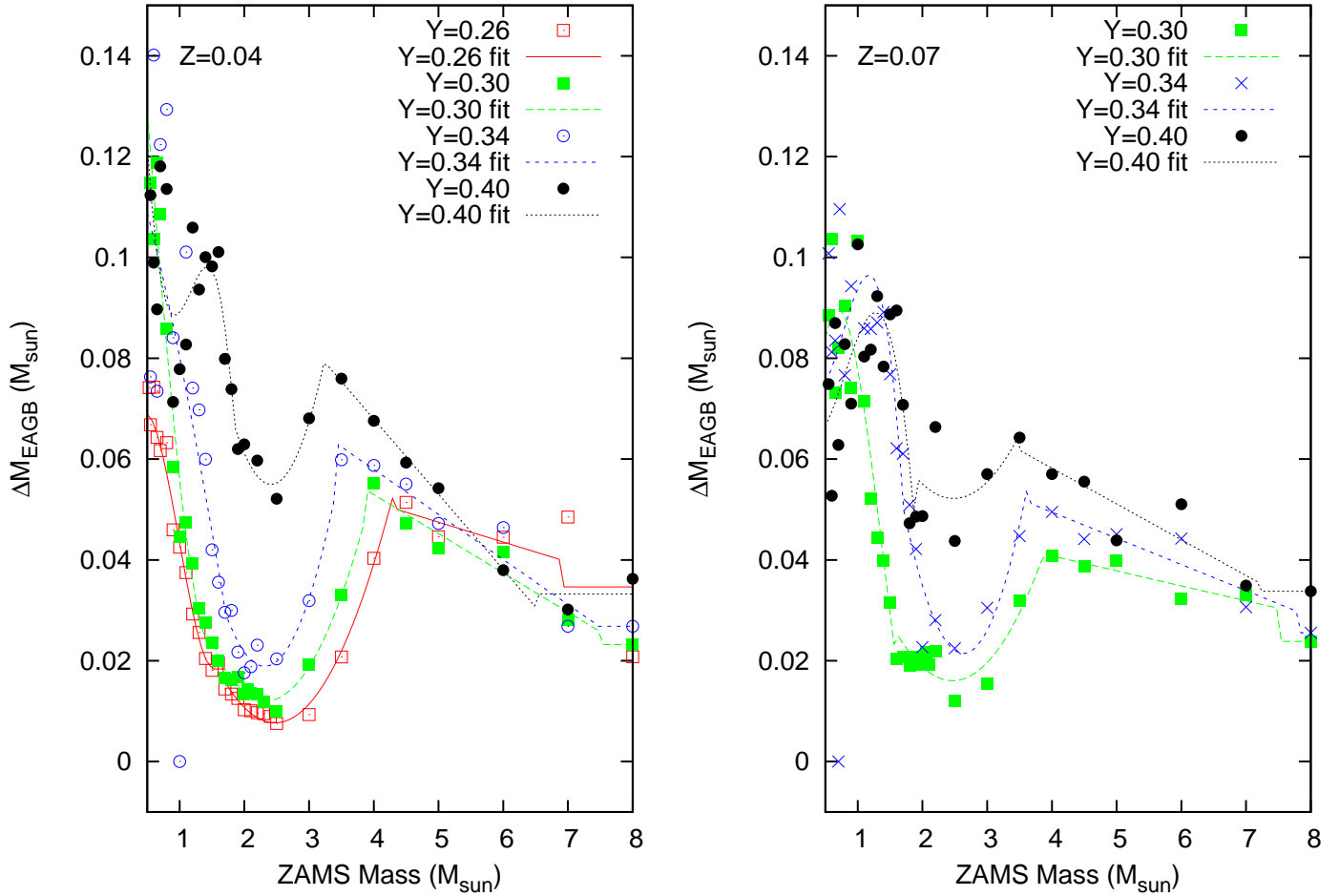


Figure 2. Each panel in the figure shows the calculated mass-loss on the early asymptotic giant branch as a function of ZAMS mass for the $Z = 0.04$ and 0.07 models for different available values of Y . The symbols and lines have the same meaning as those in Figure 1.

Table 2. Coefficients for fits to early-AGB mass-loss

Z	Y	a_{13}	a_{12}	a_{11}	a_{10}	a_{22}	a_{21}	a_{20}
0.040	0.26	0.0858588	-0.256145	0.182936	0.030799	0.0135521	-0.0670728	0.0906499
0.040	0.3	0.0435809	-0.0520068	-0.144506	0.208967	0.0154136	-0.0720782	0.0962957
0.040	0.4	-0.156291	0.552081	-0.620921	0.314167	0.0361522	-0.174489	0.265491
0.040	0.34	0.00445069	-0.0255256	-0.0266288	0.128011	0.028588	-0.13232	0.171976
0.070	0.3	0.0697326	-0.29361	0.306202	-0.00452271	0.0126149	-0.0622221	0.0927601
0.070	0.4	-0.0565319	0.135358	-0.0691988	0.0744541	0.0122269	-0.0607111	0.127542
0.070	0.34	-0.203047	0.640541	-0.631658	0.273183	0.0337056	-0.177336	0.254678

the initial helium mass fraction increases so does the mass of the core. The core mass is important since it is the most important factor controlling the luminosity of an AGB star. The core mass at the first pulse should also correlate with the resulting CSPN mass.

Figure 3 show the core mass at the first pulse from the Padova models for $Z = 0.04$ and 0.07 and $Y = 0.26, 0.30, 0.34$ and 0.40 as a function of mass. Each set of models with a given Y and Z have been fit by a double quadratic fit, one at lower masses ($\lesssim 1.5 M_{\odot}$) and one at higher masses. The transition between the two was found between 1.3 and $2.0 M_{\odot}$. The transition between the lower mass and higher

masses was determined by visual inspection of where the core mass begins to rise steeply. In all cases the fits to the points and the fit equations are yield core masses which are typically less than $0.02 M_{\odot}$ different from the calculated points.

The equations of the quadratic fits for low and high masses are given by $M_{c0,low}$ and $M_{c0,high}$. The equations are

$$M_{c0,low} = a_{12}M^2 + a_{11}M + a_{10} \quad (14)$$

$$M_{c0,high} = a_{22}M^2 + a_{21}M + a_{20} \quad (15)$$

where M is the ZAMS mass. The coefficients for the different values of Y and Z are shown in Table 3. The procedure used

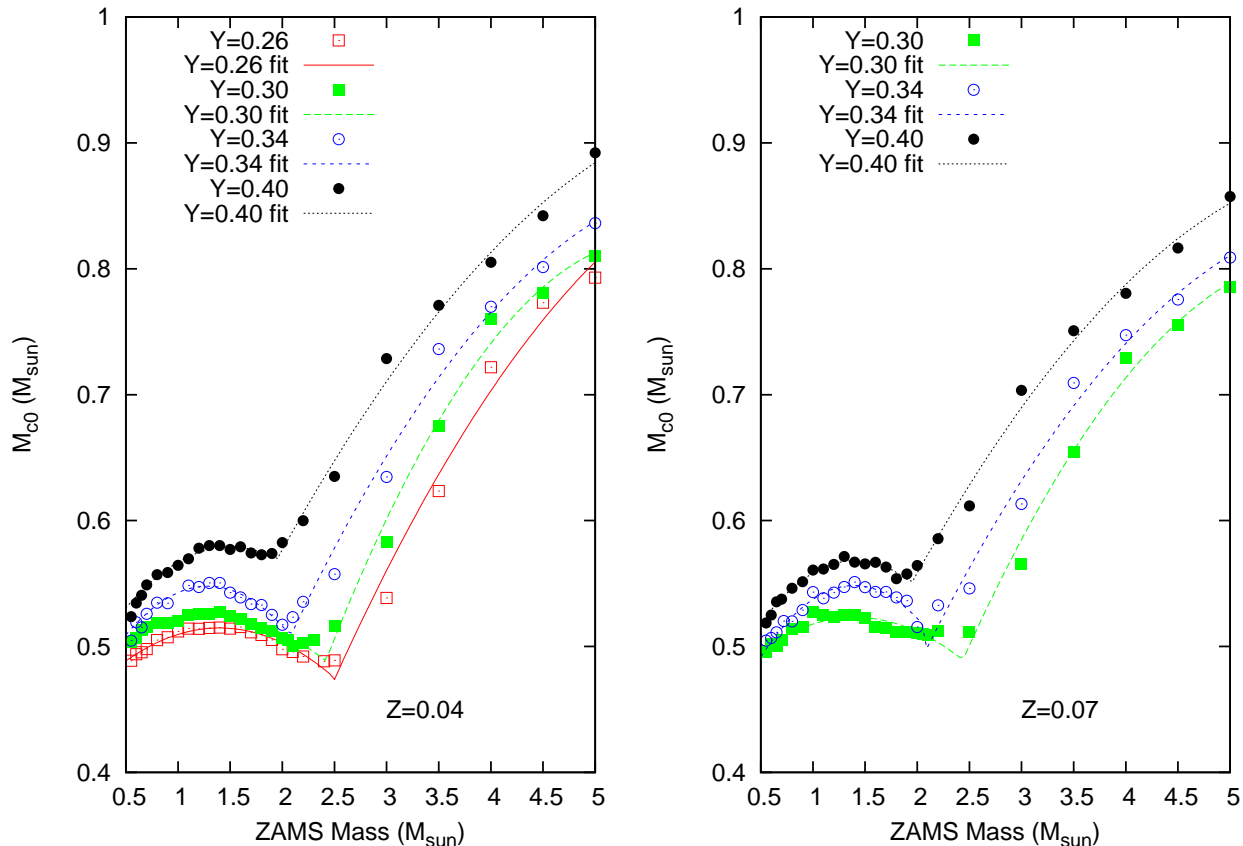


Figure 3. The figure shows the core mass at the onset of the first pulse for the $Z = 0.04$ and 0.07 models and the fits to these curves. The symbols have the same meaning as they do in Figure 1.

Table 3. Coefficients for the fits to the first pulse core masses

Z	Y	a_{12}	a_{11}	a_{10}	a_{22}	a_{21}	a_{20}
0.040	0.26	-0.0325831	0.0910294	0.451145	-0.0202143	0.284259	-0.1105
0.040	0.30	-0.0291444	0.0765474	0.473872	-0.0337214	0.375711	-0.222486
0.040	0.34	-0.0625541	0.16101	0.444288	-0.0211523	0.26243	0.0542981
0.040	0.40	-0.0483516	0.145099	0.470201	-0.015598	0.211713	0.215733
0.070	0.30	-0.0318383	0.0896357	0.45999	-0.0265214	0.314122	-0.118729
0.070	0.34	-0.071077	0.198063	0.410435	-0.0196009	0.246253	0.0692979
0.070	0.40	-0.0601748	0.169262	0.449156	-0.0167222	0.214947	0.195378

is to find the point of intersection between the two fits and then to plug in the relevant mass.

The most obvious trend is there is an increase in the core mass as the value of Y increases. This is important since on the AGB a larger core mass leads to a higher luminosity. This is also important since the mass at the first pulse is an important factor in determining the mass of the CSPN. For a constant ZAMS mass a higher ZAMS Y value should lead to a higher CSPN mass.

2.5 Third dredge-up

In synthetic AGB models the standard method to model the TDU effect is to use a dredge-up parameter λ where

$$\lambda = \frac{\Delta M_{\text{dredge}}}{\Delta M_c}, \quad (16)$$

ΔM_{dredge} is the mass dredged up and ΔM_c is the increase in the core mass during the preceding interpulse phase. During a thermal pulse the star develops a convective shell in the intershell region between the base of the hydrogen-rich envelope and just above the core. This region is helium- and carbon-rich since it consists of the products of partial helium burning. At the end of the thermal pulse the convective envelope may penetrate into this region and mix this carbon- and helium-rich material into the envelope. The parameter λ is a measure of how deeply the convective envelope penetrates into this intershell region and determines how much mass is mixed up into the outer layers.

The TDU model used in Gavilan, Buell, & Molla (2005) and Buell et al. (1997) is used. The formula to calculate λ is

$$\lambda = 0.90(\log L_{\text{He,max}} - \log L_{\text{He,min}}). \quad (17)$$

The methods to find both $\log L_{\text{He},max}$ and $\log L_{\text{He},min}$ can be found in Buell et al. (1997). $\log L_{\text{He},max}$ is the maximum luminosity of the helium shell during a shell flash and $\log L_{\text{He},min}$ is the minimum luminosity required for a dredge-up to occur. $\log L_{\text{He},min}$ is a function of the mass of the star and its value increases as the mass gets smaller. The main aspects of this formula are:

- Because the maximum luminosity of the helium shell starts below the canonical value for a given core mass typically at the first pulse this luminosity is too low to produce a dredge-up.
- The value of $\log L_{\text{He},min}$ increases as the mass decreases. This prevents TDU in the lowest mass stars.
- For the lower mass models in this paper the TDU makes only a minor contribution if it makes any to the abundances of helium and carbon. The reason is at most only 1-2 TDU events will occur and the values of λ will be small (~ 0.10).

The abundances of the dredge-up material are determined from the formulas in Renzini & Voli (1981).

2.6 Mass-loss on the TP-AGB

On the TP-AGB, mass-loss is calculated by the pulsation period-mass loss law of Vassiliadis and Wood (1993) without their correction for periods above 500 days. To make the transition from the modified Reimer's rate to this pulsation mass-loss rule the modified Reimer's rate is used until the pulsation mass-loss rule becomes larger.

2.7 TP-AGB models

The TP-AGB is followed using a synthetic AGB code which is a descendent of the Renzini & Voli (1981) code. The code begins with a guess at T_{eff} to calculate the surface boundary conditions. The equations of stellar structure are then integrated to the base of the convective envelope. The value of the effective temperature is then modified until the base of the convective envelope is at the same position as the core mass. The opacities used for high temperatures are described in Iglesias & Rogers (1996). For low temperatures the opacities of Alexander & Ferguson (1994) are used. The luminosity during the interpulse phase of the TP-AGB star is calculated using the expressions in Wagenhuber & Groenewegen (1998). A mixing length parameter, $\alpha = l/H_p$, of 1.70 is used. This value is chosen since it is close to typical values of values of α chosen for solar models.

3 PARAMETERS OF THE GALACTIC BULGE PLANETARY NEBULA

3.1 Metallicity, oxygen and helium abundances

Before trying to match stellar models to the global parameters and abundances of GB-PNe, it is necessary to decide what values of these parameters should be matched. Figure 4 shows $\log(\text{O}/\text{H})+12$ as a function of He/H for five different GB-PNe abundance data sets: the set of Cuisinier et al. (2000) (Cuisinier set), the set of Escudero, Costa & Maciel (2004) (Escudero set), the set of Exeter, Barlow & Walton (2004) (Exeter set), the set in Liu et al. (2001) and

Wang and Liu (2007) (Wang & Liu set), and the set in Ratag et al. (1992) and Ratag et al. (1997) (Ratag set). For all sets the abundances of all elements except He/H are the values reported by the authors of their analysis of collisionally excited lines (CELs). The Wang & Liu papers also report heavy element abundances from optical recombination lines (ORLs). These are not used since the abundances from ORLs are different from the abundances from CELs and are generally considered to be less reliable (A review of the reliability and the origin of ORLs can be found in (Liu 2006)). For all of the sets the helium abundances are the values reported by the authors from ORLs.

Overall each of the data sets seem to agree with each other, however, there are some important differences. Most of the points from the different sets seem to fall in the same area on the graph. For He/H values between ~ 0.08 and ~ 0.14 the values of O/H for all of the sets overlap although some of the sets have a larger scatter. The Escudero and Ratag sets have the largest scatter in O/H and the Cuisinier and Wang & Liu sets have the smallest. The biggest difference is both the Escudero and Ratag sets have a tail of GB-PNe with He/H greater than 0.16, whereas, the other sets do not.

What is the origin of the high He/H tail in Figure 4? In this figure for $\text{He}/\text{H} \gtrsim 0.150$ the value of O/H decreases from a maximum and appears to level out into a tail. This tail is composed of PNe from only two of the sets, the Escudero and Ratag sets. Since this tail does not show up in the other sets, this suggests the most likely explanation is due to either differences in how PNe were selected or how the abundances are computed. The abundances for all five sets were computed using similar sets of ionization correction factors and they produce very similar results in the He/H range of 0.08 to 0.14. This suggests the differences arising from the methods of calculating the abundances are small. This does not rule out errors in computing He/H as an explanation. A possible origin of this tail is in the GB-PNe selection criteria. The different sets use different methods to determine what is a likely GB-PNe. For example for the Cuisinier set the criteria for a PN to be in the bulge are (i) its diameter must be smaller than 10 arcsec, (ii) it must be within 5 degrees of the galactic centre, and (iii) the 6cm radio flux must be less than 100 mJy. The Escudero set selected for GB-PNe as PNe within 5 kpc of the centre. This is a less discriminating criteria and as a result a larger fraction of the Escudero set being disc PNe. Escudero, Costa & Maciel (2004) estimates ~ 20 percent of their sample is disc PNe. A possible explanation of the tail is it consists of inner disc PNe from intermediate-mass progenitors. For purposes of modeling it will be assumed this tail is not real since it should show up in all five sets.

There are a couple of possibilities if this tail is real bulge population. One possibility is it is produced by low-mass progenitors with $Y \sim 0.4$. This is not unprecedented since some globular clusters may contain a third, even more helium rich (extreme) population. Another alternative is these PNe would be the progeny of galactic bulge blue straggler stars (Clarkson et al. 2011). The blue stragglers in the bulge with an assumed MSTO at $1.4 M_{\odot}$ could be as massive as $2.8 M_{\odot}$. Stars of that mass would experience many TDU events which would enhance the abundances of helium and carbon; this could explain the high He abundances. Blue

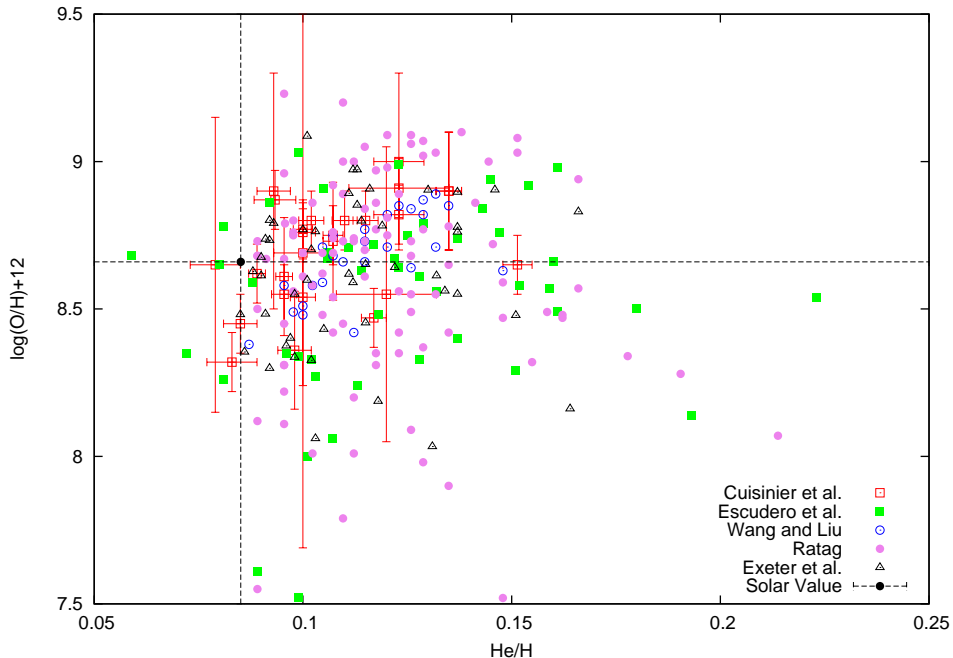


Figure 4. The figure shows abundances of $\log(\text{O}/\text{H})+12$ as a function of He/H . The red open squares, green filled squares, blue open circles, violet filled circles and black open triangles are from the GB-PNe data from (Cuisinier et al. 2000) (Cuisinier set), Escudero, Costa & Maciel (2004) (Escudero set), Liu et al. (2001) and Wang and Liu (2007) (Wang & Liu set), Ratag et al. (1992, 1997) (Ratag set), and Exeter, Barlow & Walton (2004) (Exeter set), respectively. For reference the solar values of Asplund, Grevesse, & Sauval (2005) are indicated by the dashed lines.

straggler models for the tail would probably also require enhanced helium abundances since material from the interior of the star being consumed would end up near the surface.

Is there a relationship between O/H , which stands in for metallicity, Z , and He/H which stands in for the helium mass fraction, Y ? In Figure 4, by visual inspection, it appears that as O/H increases so does He/H in the range of He/H of 0.08-0.14. This trend is much clearer in Figure 5 where only the sets with the smallest scatter, the Cuisinier set and Wang & Liu sets, are plotted. In Figure 5 there is a clear trend that as O/H gets larger so does He/H in the He/H range from 0.08 to 0.135. The Escudero and Exeter sets do not show as a clear relationship between O/H and He/H as the Cuisinier and Wang and Liu sets. However, both sets are consistent with there being a relationship between O/H and He/H , as there appears to be an upward trend in both. The Ratag sample is noisier than the other samples, but it is consistent with there being a relationship between O/H and He/H .

An important point to note is there may be a systematic difference between the abundances of oxygen as determined from unevolved stars and PNe. Chiappini et al. (2009) compared the oxygen abundances of GB-PNe determined from CELs to the oxygen abundances determined from giants and found the PNe abundances are systematically lower by 0.3dex. The origin of this shift is not clear since dust should,

at most, decrease the abundance by ~ 0.1 dex. It is not clear if this shift is real or not so the models in 4.4 will look at both possibilities.

Does O/H actually trace O/H of the progenitor star? The abundance of oxygen in a PN should be close to but not identical to the progenitor ZAMS abundance, since oxygen should experience a slight decrease (typically a few percent) in abundance during the FDU at low masses. At higher masses, which we will not look at in this paper, oxygen is decreased by the SDU and HBB. Oxygen can be increased in TDU events. However, all of these changes cause only minor changes in the abundance of oxygen, so the oxygen abundance in PNe should be a good indicator of the ZAMS oxygen abundance even with high mass progenitors.

Additional support for the proposition He/H increases with metallicity comes from plotting He/H against heavy elements other than oxygen. Figure 6 shows Ne/H , S/H , Cl/H and Ar/H as a function of He/H . This figure shows clearly for all the sets abundances of Ne, S, Cl and Ar increase with He/H up to $\text{He}/\text{H} \sim 0.14$. None of these elements is thought to be significantly effected by the stellar evolution between ZAMS and the PN stages. Neon and argon have an additional advantage, because they are noble gases, their abundances will not be affected by being drained onto dust grains, although for the other elements this effect is proba-

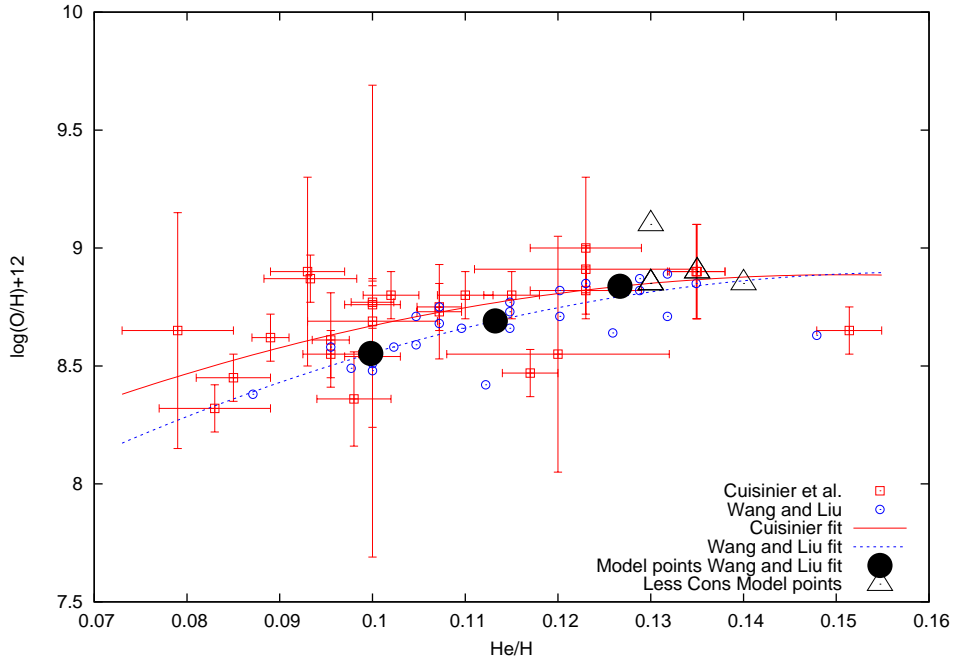


Figure 5. This figure is the same as Figure 4 but with only the Cuisinier and Wang & Liu sets only. The solid and dotted lines are respectively the fits to the Cuisinier and Wang & Liu set. The large filled circles are the parameters fit by TP-AGB stars modeled to the Wang & Liu fits in 4.1. The large open triangles are the positions of fits of additional models in 4.2, 4.3, and 4.4. See the text in Section 4 for an explanation.

bly small. This figure suggests as the metallicity of the star increases so does the value of He/H. For all four elements the abundances increases with He/H up to He/H \sim 0.14. There is a tail at high He/H where these abundances drop off. This is the same pattern as seen for the relationship between the abundance of oxygen and He/H. The high He/H tail show up in each graph where the Escudero and Ratag sets were plotted. As noted above its existence is questionable.

In this paper it is assumed the most metal rich PNe are due to the youngest progenitors. These youngest and most massive progenitors seem to have a PN He/H between 0.130 and 0.140 and the abundance of oxygen is in the range 8.80-8.90. If we accept the potential systematic upward shift of the oxygen abundance by 0.3dex then the oxygen abundance could be approximately 9.10-9.20 for the most metal rich PNe. In Section 4 these will be the abundances of the most massive GB-PNe matched.

Does it matter if there is a injective relationship between metallicity and He/H or if there is a spread of metallicities for the same Y value? The answer is no since there are a significant number of GB-PNe with He/H \approx 0.14 in all five sets which require some explanation. The Y values of PNe can be estimated from the following formulas

$$X + Y + Z = 1 \quad (18)$$

and

$$\frac{Y}{X} = 4\text{He}/\text{H}. \quad (19)$$

A maximum Y values can be estimated by assuming the GB-PNe with the highest He/H have $Z = 0.02$. In this case for He/H=0.140 the formulas above give $Y \approx 0.35$. Different, but reasonable assumptions about Z would not appreciably change Y . Clearly the GB-PNe span a significant range of possible Y and Z values.

In this paper it is assumed that each value of the progenitor Z gives a unique value of Y . To get a relationship between O/H and He/H quadratic fits have been made in Figure 5 to the Cuisinier set and the Wang & Liu set. The fit to the Cuisinier set is given by

$$\log(O/H)+12 = -103.981(\text{He}/\text{H})^2 + 32.4351(\text{He}/\text{H}) + 6.35192. \quad (20)$$

The fit to the Wang & Liu set is given by

$$\log(O/H)+12 = -97.2275(\text{He}/\text{H})^2 + 30.9835(\text{He}/\text{H}) + 6.42915. \quad (21)$$

If He/H=0.130 the value of O/H is respectively 8.81 and 8.81, respectively, for the Cuisinier and the Wang & Liu sets. At He/H=0.09, O/H is respectively 8.43 and 8.43 for the Cuisinier and the Wang & Liu sets. Some of the models of the PNe global parameters from models will be made along these fits but some fits will be made away from these curves.

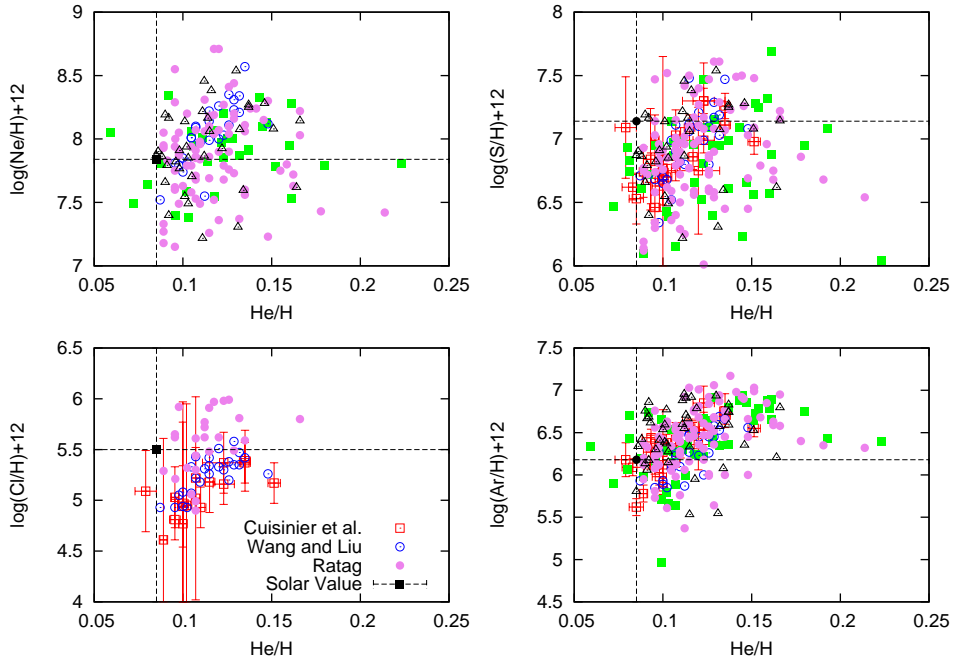


Figure 6. The figure shows abundances of $\log(\text{Ne}/\text{H})+12$, $\log(\text{S}/\text{H})+12$, $\log(\text{Cl}/\text{H})+12$, and $\log(\text{Ar}/\text{H})+12$ as a function of He/H . The symbols have the same meaning as they do in Figure 4.

3.2 Central star masses of GB-PNe

The mass of the central star of a PN (CSPN) is critical for determining the mass of the progenitor. Both observational (Weidemann 1977, 2000; Kalirai et al. 2005; Catalán et al. 2008) and theoretical studies (Dominguez et al. 1999; Marigo 2001; Meng, Chen, & Han 2008) indicate there is a link between the mass of the progenitor and the mass of the resulting white dwarf. The expected theoretical relationship is qualitatively confirmed by the observational studies which show the larger the mass of the progenitor the larger the mass of the resulting white dwarf. Theoretical studies indicate the initial-final mass relationship (IFMR) should depend on metallicity. In particular, the smaller Z is the larger the resulting white dwarf for any given ZAMS mass. Any potential metallicity relationship is less clear in the observational studies (Catalán et al. 2008) as there is considerable scatter in the observational IFMR. Other factors such as stellar rotation may also affect the IFMR (Dominguez et al. 1996; Catalán et al. 2008).

In Paper I it was predicted there should be a difference in the IFMR for different ZAMS value of Y . Given the same mass and metallicity a higher value of Y gives a higher core mass at the onset of the first thermal pulse. Since the core mass at the first pulse is correlated to the CSPN mass, a higher Y on the ZAMS should lead to a larger CSPN mass.

There do not appear to be a large number of recent studies on the CSPN masses of GB-PNe. The existing studies are

consistent with the expectation the bulge contains mostly low-mass ZAMS progenitors. Tylanda et al. (1991) used a variety of methods to get the CSPN mass; this included plotting the Zanstra luminosities of PNe, $L(\text{HI})$ and $L(\text{HeII})$ as functions of the respective Zanstra temperatures, $T(\text{HI})$ and $T(\text{HeII})$. These were compared to the theoretical CSPN tracks of Schönberner (1981, 1983) to get the CSPN masses. Tylanda et al. (1991) also compared the visual magnitudes of the CSPN to the expansion ages and the temperatures to their f parameter to get CSPN masses. They got an average mass of the Galactic bulge CSPN of $0.593 \pm 0.025 M_{\odot}$. Their Figures 11 and 12 present the CSPN mass distribution of all their masses and all the best determined masses, respectively. There is a peak in both figures of the number of CSPN masses at $\sim 0.58 M_{\odot}$. The distributions tails off quickly to $0.65 M_{\odot}$. About 10 percent of their sample have masses greater than $0.62 M_{\odot}$ in their sample. This is nearly the same as their estimate of the number of disc objects contaminating the sample (Stasińska et al. 1991). The high mass tail could be due to sample contamination by foreground objects or could be due to blue stragglers in the bulge. This study suggests the highest mass CSPNs have masses between 0.58 and $0.62 M_{\odot}$.

Ratag (1991) determined the luminosities and temperatures by two methods. The first is a version of the Zanstra method which adds in the energy from the far infrared part of the spectrum to get the stellar temperature and the luminosity. The second is a method using an photoionization

model where important line ratios were matched to observations to get the spectral distribution of the stellar continuum. The stars' effective temperature is derived from the continuum. The luminosity in the second method is determined by adding the energy from all emission lines, the free-free emission and the infrared luminosity and the portion of the stellar spectrum emitted with wavelength less than 91.2 nm. The agreement between the luminosities and temperatures determined by various methods is pretty good (See Figure 2 and Figure 4 in Ratag 1991 Chapter 4 for these comparisons.).

Ratag 1991 plotted these luminosities and temperatures on HR diagrams with theoretical tracks. This figure is partially duplicated in Figure 7. Almost all the Ratag PNe fall between the $0.546 M_{\odot}$ and the $0.644 M_{\odot}$ tracks. However, the majority falls between $0.546 M_{\odot}$ and $0.600 M_{\odot}$. This suggests the most massive GB-PNe CSPN are between 0.58 and $0.60 M_{\odot}$. This is consistent with the Tylanda et al. (1991) results.

Both the Tylanda et al. (1991); Ratag (1991) results suggest that the progenitors of the GB-PNe are relatively low-mass since the observed CSPN masses are low. Both of these studies are quite old and neither has been repeated recently so some skepticism is justified. However, the distance to the bulge is relatively well known and the intensity of the radiation from the GB-PNe can be measured with some confidence. Many of these PNe appear to fall on the horizontal part of the CSPN tracks. Since the luminosities, which are nearly constant in this region, can be fairly well constrained, the CSPN masses should be reasonably accurate ($\Delta M_{\text{CSPN}} \sim 0.03 M_{\odot}$).

Some additional support for a low maximum bulge CSPN masses comes from the luminosity of the tip of the AGB branch. Zoccali et al. (2003) found the maximum bolometric magnitude of the AGB tip is -5.0 which corresponds to a luminosity of about $8000 L_{\odot}$ ($\log L \approx 3.9$). In Figure 28 of Zoccali et al. 2003 most of the stars at the tip of the AGB are closer a bolometric magnitude of -4.5 which corresponds to a luminosity of about $5000 L_{\odot}$ ($\log L \approx 3.7$). If you compare these luminosities to the horizontal parts of the CSPN tracks of Blöcker (1995) this implies a CSPN mass $\sim 0.605 M_{\odot}$ track. Therefore, the AGB tip luminosity suggests the majority of the CSPNs have masses less than $0.61 M_{\odot}$.

Putting all of the evidence together suggests the most massive CSPN PNe in the bulge are between 0.58 and $0.62 M_{\odot}$. Therefore, for the purpose of model fitting in this paper, it is assumed all the masses of the CSPN of GB-PNe are less than or equal to $0.620 M_{\odot}$. This maximum mass may be less than $0.600 M_{\odot}$.

Another study which looked more recently at the question of bulge CSPN masses is Hultsch et al. (2007). In this study the spectra of the central stars of a small sample of GB-PNe was obtained. From these the abundances, the effective temperatures, and the surface gravities were obtained. The effective temperature and surface gravity were compared to theoretical tracks to get the CSPN mass. Using this method a higher average mass is obtained for their small sample (5 objects) of PNe of $0.696 M_{\odot}$, which is higher than studies which measure the effective temperature and luminosity using the nebula. Two of the GB-PNe have a mass of nearly $0.800 M_{\odot}$ which implies intermediate-mass

progenitors ($M \gtrsim 3.5 M_{\odot}$). There is reason to be skeptical of this though. As the authors note, if their inferred luminosities are used to find the distance to the Galactic bulge is 10.7 ± 1.2 kpc. This distance which is 25 percent larger than the typical determination, e.g. 8.4 ± 0.4 kpc (Ghez et al. 2008).

What is the relationship between the helium abundance and the CSPN mass of the the GB-PNe? In Figure 8 the five different samples of GB-PNe He/H are plotted as a function of their CSPN mass from Tylanda et al. (1991). Visual inspection of this figure indicates there is a lot of scatter in all sets but the graph is consistent with an upward trend between 0.55 and $0.62 M_{\odot}$. If there is an upward trend it appears to end between 0.60 to $0.63 M_{\odot}$. The lack of a significant correlation could be due to the relatively large errors expected in the individual CSPN masses. A positive correlation between He/H and CSPN mass would be expected if as might be expected in any typical chemical evolution model where the ISM is being simultaneously enhanced in both helium and metals. Therefore the more massive CSPN should have higher values of Y and Z .

At even higher core-masses it appears the value of He/H drops off into a tail with a relatively modest He/H (~ 0.110). Is the high CSPN core mass ($\gtrsim 0.62 M_{\odot}$) tail real effect in the bulge or is it due to disc PNe contamination? Although this paper can not definitively answer this, the fact most of the sets have similar He/H in the tail part of the distribution suggests the tail may be real. What might cause this tail? If it is real then one possibility is these are foreground objects misidentified as bulge objects. If they are disc objects they would appear more luminous and thus more massive. If they are foreground objects then these PNe would have values of He/H typical of the disc PNe ($\text{He}/\text{H} \approx 0.110$). Another possibility is these objects are the progeny of blue straggler star in the bulge. Potential blue stragglers have recently been identified in the bulge and the progeny of these more massive stars would be more massive CSPN.

To get a better look at the relationship between core mass and He/H from the various GB-PNe of the Escudero set and the Wang & Liu set are plotted as a function of CSPN mass, where the CSPN masses are from the best set from the Tylanda et al. 1991 paper (as identified in that paper), in Figure 9. Both of these sets seem to show as CSPN mass increases so does the value of He/H. This does not mean there is a unique relationship between CSPN mass and He/H. Only the fit to the Wang & Liu set has a truly significant correlation coefficient. The lack of a definite relationship could be due to the significant scatter in the CSPN masses.

Although there is possibly no unique relationship between He/H and CSPN mass this paper will assume there is one. The Wang & Liu set seems to have the clearest relationship between He/H and CSPN mass. The fit to the Wang & Liu set is given by

$$\text{He}/\text{H} = 0.671821(M_{\text{CSPN}} - 0.60) + 0.113244. \quad (22)$$

This equation will be used to derive the parameters to be fit in Section 4.1.

In Figure 7 the Ratag sample is separated into two samples with high He/H (> 0.120) and low He/H (< 0.120) and plotted on the HR diagram using the Ratag values of $\log L$ and $\log T_{\text{eff}}$. This is done since this gives a larger set of

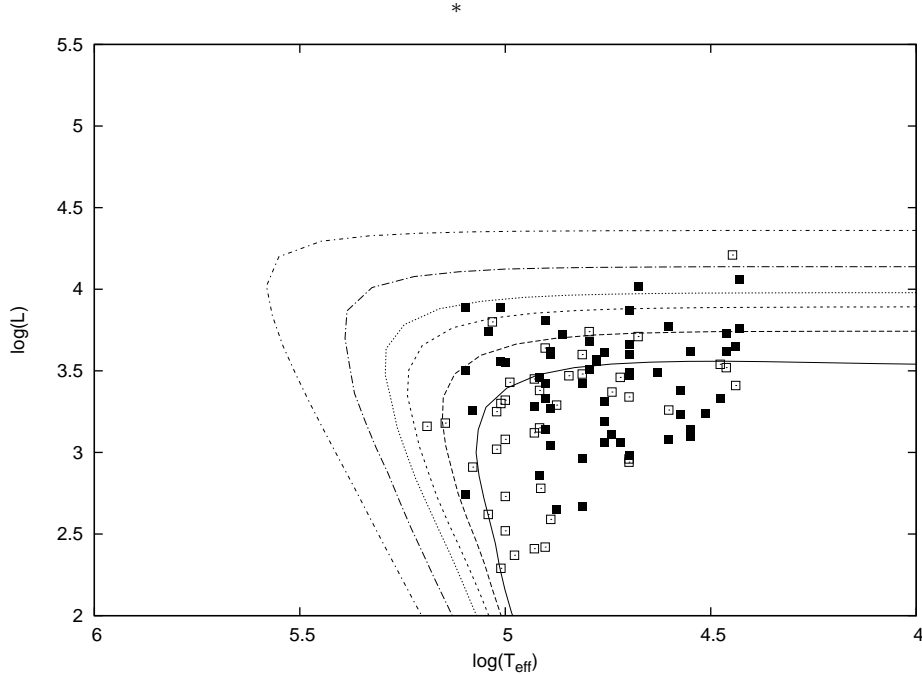


Figure 7. This figure shows the positions of the Ratag set on the HR diagram with the theoretical Vassiliadis and Wood (1994) put in for comparison. The filled squares are the PNe with $\text{He}/\text{H} < 0.120$ and the open squares are the PNe with $\text{He}/\text{H} > 0.120$. The solid, long dashed, short dashed, dotted, long dash-dot, and short dash-dot are the theoretical tracks of 0.569, 0.597, 0.633, 0.677, 0.754, and 0.900 M_{\odot} . All the tracks have ZAMS $Z = 0.016$.

CSPN masses than the Tylenka et al. 1991 CSPN masses. Visual inspection reveals there is at most a minor difference in the distribution on the HR diagram of the two subsets. More of the high He/H GB-PNe seem to fall on the cooling part of the tracks. This indicates the high He/H PNe a slightly higher CSPN mass, since more massive CSPN evolve more quickly (e.g. see Vassiliadis and Wood (1994)). This makes it more likely more massive CSPN will end up on the cooling part of the tracks.

3.3 Helium versus N/O in GB-PNe

Nitrogen is a very important element in PNe since it is often used as an indicator of nuclear processing of material in the interior. This material is then transported to the surface via convection. In low and intermediate-mass stars nitrogen is typically enhanced at the FDU and SDU. Nitrogen can also be enhanced when CNO process occurs at the base of the convective envelope in AGB stars, known as HBB.

Bulge stars are thought to be fairly low-mass, the work of Bensby et al. (2010, 2011) suggests the youngest stellar ages are ~ 3 Gyr of age which would suggest a maximum MSTO mass of $\sim 1.5 M_{\odot}$. Stars of this mass should only experience the FDU which has only a limited effect on N/O, typically doubling N/O, which is an increase of about 0.3 dex. For a ZAMS star with a solar ratio of N/O this would

mean N/O would be around 1/3 ($\log(\text{N}/\text{O}) \approx -0.5$) in a PNe.

In Figure 10 the ratio of N/O of GB-PNe is plotted as a function of the ratio He/H for all five sets. There is clearly a relationship between N/O and He/H for GB-PNe, with both increasing at the together in all of the sets. A fit to the Wang & Liu set, which is shown on the figure gives:

$$\log \text{N}/\text{O} = 15.25(\text{He}/\text{H} - 0.100) - 0.755. \quad (23)$$

This line appears to be a good fit to all of the data sets. It will be adopted to determine the GB-PNe N/O parameter to match in some cases.

Of particular importance is the fact the highest N/O ratios are $\lesssim 1$ in almost all of the sets. The Cuisinier and Wang & Liu sets all of the GB-PNe have $\text{N}/\text{O} \lesssim 1$. For the Exeter set with the exception of two clear outliers with $\text{N}/\text{O} \approx 10$, all the GB-PNe N/Os in their sample are $\lesssim 1$. The Escudero set has only a two PNe with N/O significantly larger than 1. Only the Ratag set has a significant number of GB-PNe with $\text{N}/\text{O} \gtrsim 1$. For purposes of this paper it will be assumed for GB-PNe $\text{N}/\text{O} < 1$ since all sets have points in this range and most of them do not have a significant number of GB-PNe with N/O significantly larger than 1.

An N/O of ~ 1 suggests either the progenitors are intermediate-mass or else are low-mass with a higher than solar N/O ratio, 0.13. The second is very interesting since it would suggest the gas from which these stars formed was en-

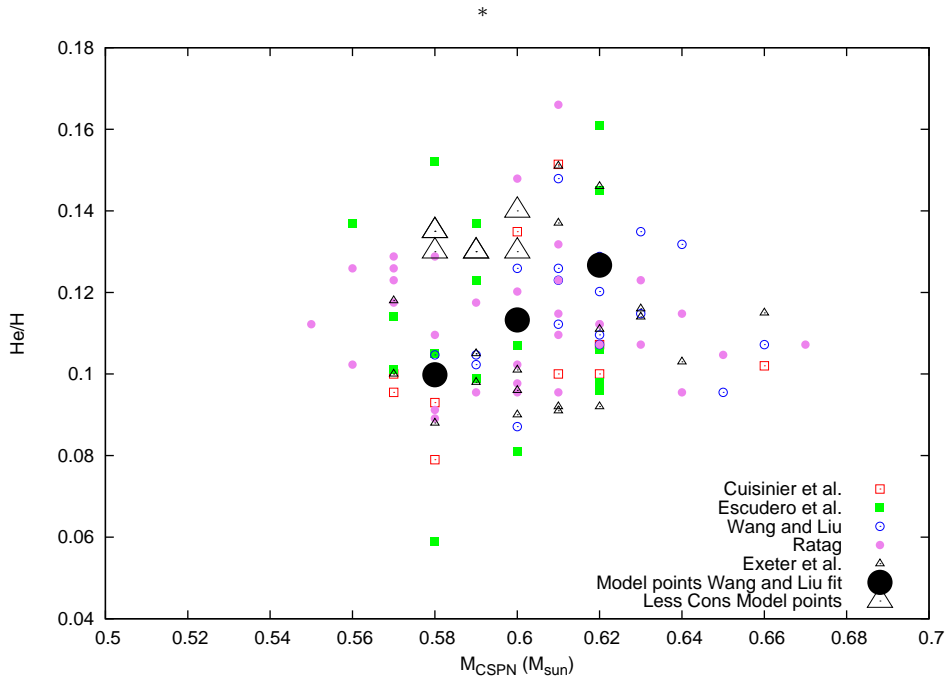


Figure 8. The figure shows the value of He/H for GB-PNe versus the central star mass from Tylenda et al. (1991). The symbols have the same meaning as in Figure 4. The large filled circles and large open triangles have the same meaning as in Figure 4

hanced in both helium and nitrogen. This would indicate the bulge ISM was enhanced by the products of CNO burning.

3.4 Carbon in GB-PNe

Another very important element is carbon. Information about this element for GB-PNe is limited because the bulge is heavily reddened, and the most reliable lines for determining the carbon abundance in PNe are in the ultraviolet. The Wang & Liu set contains a limited number of measurements of the ratio of C/O from both CELs and ORLs. Most of their C/O ratios from both methods are below 1 but there are a small number with C/O > 1 which could indicate TDU events. This is consistent with the findings of Gutenkunst et al. (2008); Perea-Calderón et al. (2009); Stanghellini et al. (2012) who found the majority of GB-PNe have oxygen-rich dust spectrum but there is a minority of stars (≈ 10 percent) which have carbon-rich dust spectrum. A large fraction (≈ 40 percent) of GB-PNe have a mixed dust spectrum with both carbon and oxygen features. The mixed features may be associated with a TDU event occurring near or after the transition from an AGB star to a PN, but it may also be due to a dense torus around the progenitor where, during the transition from the AGB to PN phases, chemical reactions occur in an oxygen rich environment which produces poly-aromatic hydrocarbons (PAHs). This PAH production shows up as the carbon-features in a

mixed dust spectrum (Guzman-Ramirez et al. 2011). In the second scenario a mixed feature spectrum does not necessarily indicate a carbon-rich star in which a TDU occurred.

The conclusion is the majority of progenitors of GB-PNe do not experience a TDU event. This is supported by the lack of bright carbon stars in the bulge (Azzopard, Lequeux and Rebeiro 1988). This indicates the carbon stars in the bulge which do exist probably formed as the result of a mass transfer in a binary system and not by the action of the TDU. This further supports the idea that the stars in the bulge are older, since only stars with $M \lesssim 1.6 M_{\odot}$ do not experience a TDU.

There may be some indication that a minor amount of TDU occurs. Uttenthaler et al. (2007) observed Tc in bulge AGB stars which is an indication of the action of the TDU. In their spectra Tc was only observed in the brightest and reddest stars with the longest periods indicating they are probably the most evolved and closest to the transition to the PN phase. This suggests that the youngest stars in the bulge may be just massive enough to experience one or two dredge-ups before entering the PN phase. Depending on the mass of the residual envelope an AGB star could become a carbon star at the last moment. This would agree with the small number of GB-PNe with C/O > 1. From their luminosities Uttenthaler et al. 2007 concluded that the progenitors of these Tc rich stars are $\approx 1.5 M_{\odot}$.

All indications are the TDU plays only a minor role in

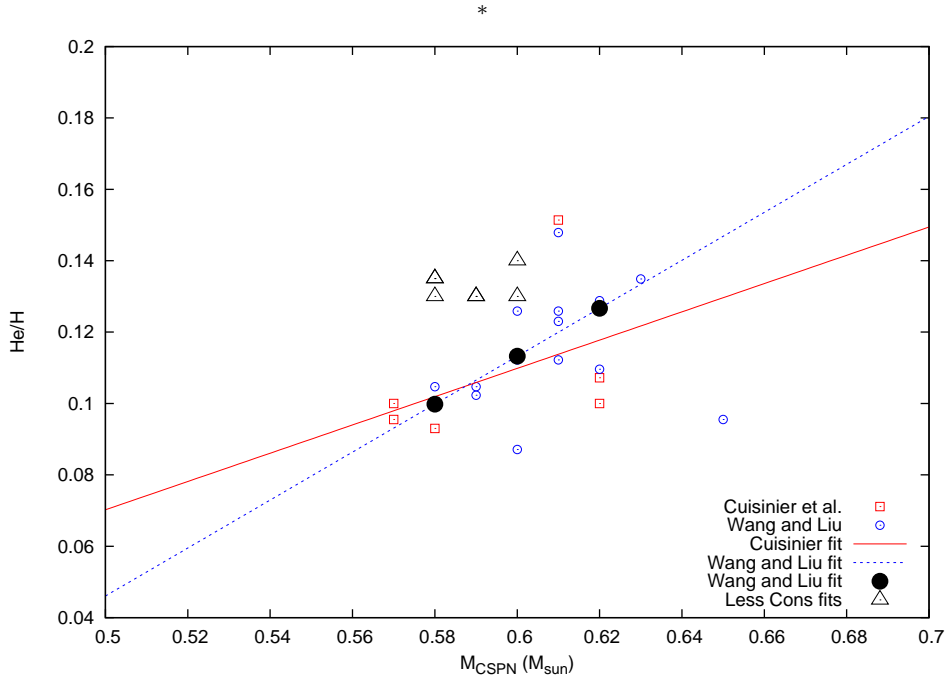


Figure 9. The figure is the same as Figure 8 but only the Cuisinier and Wang & Liu sets are plotted against the best CSPN masses of Tylenda et al. (1991). Linear fits to both sets are shown to make the trends are clear.

modifying the abundances in PNe. This is important since the TDU can significantly modify the abundance of helium but it takes several TDU events to significantly modify it. Therefore, He/H for these lower mass models is mostly a function of the initial value of He/H and the result of the FDU. It will be assumed for fitting purposes, the C/O for GB-PNe is less than 1.

4 RESULTS

In the previous section it was noted there are a range of possible GB-PNe parameters to fit. In this section models are calculated which fit different potential but reasonable parameters of the highest mass CSPN. The first set of GB-PNe parameters fit in this paper is defined by the Wang & Liu fits. This set shows the most well defined trends and it seems to be a reasonable fit. After that this paper will look at some less conservative possibilities where the maximum bulge CSPN mass is less than $0.62 M_{\odot}$.

The basic fitting technique is as follows. A set of typical PNe parameters to fit is chosen. These parameters are the assumed CSPN mass and the PNe values of He/H, O/H, and N/O. The ZAMS mass, [Fe/H], Y and N/O were chosen and a model run. The ZAMS parameters were modified until a fit to the PNe parameters was achieved.

4.1 Wang & Liu set

In this subsection models are matched to points on the fits to the Wang & Liu set. These fits were chosen since this set shows the most well defined trends. There is also a defined trend in CSPN mass, which will be used to explore the chemical evolution of the bulge. Table 4 shows the PNe parameters fit, the ZAMS parameters of the best fitting models. The positions of the GB-PNe parameters to be fit are indicated in Figures 5, 10 and 9. In these fits the most massive CSPN fit have a mass of $0.62 M_{\odot}$. This probably too high maximum CSPN mass will produce the largest bulge progenitor mass. The top of the trend was fixed at a CSPN mass of $0.62 M_{\odot}$ in the fits to the Wang & Liu GB-PNe this will produce an He/H ≈ 0.130 which is similar to the maximum He/H in GB-PNe as defined in Subsection 3.1. The lowest mass models have a CSPN mass of $0.56 M_{\odot}$.

To produce the highest mass CSPN a model with $M \approx 1.8 M_{\odot}$, $Y = 0.32$ and $Z = 0.0175$ is required. The approximate age of a 1.8 solar mass $Y = 0.32$ and $Z = 0.0175$ star is about 2 Gyr. This is a higher mass and younger age than indicated by the work of Bensby et al. (2010, 2011), where their largest mass is $1.25 M_{\odot}$ with an inferred age of 2.9 Gyr. This should be considered an upper limit on the ZAMS mass.

However, an initial mass of $1.8 M_{\odot}$ would be enough to produce a small number of luminous carbon stars. In this grid of model stars the $1.8 M_{\odot}$ star experiences a TDU event at the last pulse. This TDU increases the carbon abundance

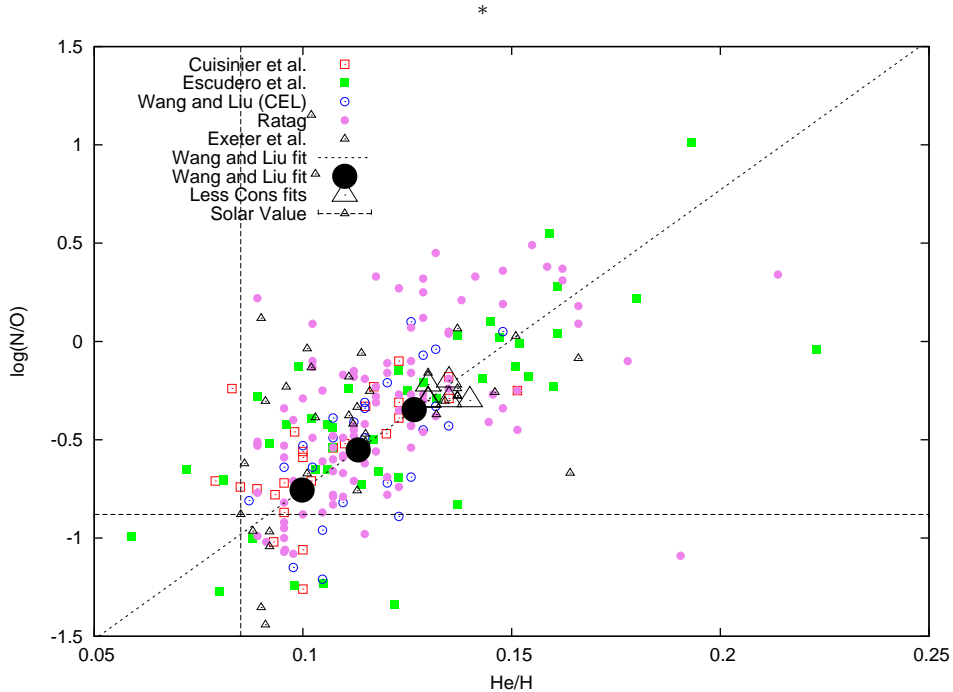


Figure 10. This figure shows the positions of the values N/O as a function of He/H for the GB-PNe. The symbols have the same meaning as in Figures 4 and 5.

Table 4. Parameters to fit and parameters of model fit for Wang & Liu set

CSPN mass	He/H	$\log(\text{O}/\text{H})+12$	$\log(\text{N}/\text{O})$	M	Y_{ZAMS}	Z_{ZAMS}	[Fe/H]	$\log(\text{N}/\text{O})_{ZAMS}$
0.58	0.09981	8.553	-0.559	1.43	0.257	0.0087	-0.18	-0.800
0.60	0.11324	8.691	-0.400	1.63	0.293	0.0122	0.003	-0.630
0.62	0.12668	8.794	-0.347	1.80	0.320	0.0175	0.195	-0.573

The CSPN mass, He/H, $\log(\text{O}/\text{H})+12$, and $\log(\text{N}/\text{O})$ are the PN parameters being fit. M, Y_{ZAMS} , Z_{ZAMS} , [Fe/H] and N/O_{ZAMS} are the model ZAMS parameters of the best fitting model. In all of these models the parameter $k_1=[\alpha/\text{Fe}]$ is set as +0.35. The end of the alpha plateau, $k_2=[\text{Fe}/\text{H}]$, is set to -1.

slightly but does not raise the ratio of C/O above 1. This is consistent with the deficit of bright carbon stars in the bulge. A single dredge-up would be sufficient to bring an observable amount of Tc and other s-process elements to the surface. Any carbon stars that form would do so when the last pulse is close to the time when the envelope is ejected. The smaller the mass of the envelope, the easier it is to pollute with dredged-up material. The carbon star lifetime would be short in this case and this would explain the lack of luminous carbon stars. The inferred maximum mass would also not be sufficient to produce stars which undergo HBB and/or SDU.

The inferred model value of [Fe/H] for the highest mass models is +0.195. This is reasonably close to the maximum values found by Bensby et al. 2010. They found in their sample of bulge main sequence and subgiant stars a bimodal distribution of [Fe/H], one with a low and one with a high

[Fe/H]. In their group with the highest values of [Fe/H], the range of [Fe/H] is between +0.10 and +0.56 with a peak at +0.3. The differences between the [Fe/H] found in this fit and Bensby et al. (2010) are small and can be reconciled by a different choice of the level of the alpha plateau in this paper. In Bensby et al. 2011 Figure 10 it appears the [O/Fe] plateau is closer to +0.5 then to +0.35 as chosen by this paper. It is important to note that other alpha elements are closer to the +0.35 plateau. With a higher plateau value the downward slope of [O/Fe] is steeper. In this case for the PNe models to match the O/H value a higher [Fe/H] value is required.

Another problem with this model is this produces an AGB star tip luminosity ($M_{bol} = -5.14$) which is more luminous than observed compared to what is seen in Zoccali et al. (2003) ($M_{bol} \approx -4.6$). This is not surprising since TP-AGB stars are expected to follow a core-mass lumi-

nosity relationship. As noted in Subsection 3.2 the maximum CSPN mass is probably less than $0.62 M_{\odot}$.

This model is in qualitative but not quantitative agreement with observations of the bulge. It is in qualitative agreement because the overall features of GB-PNe are reproduced, it matches the observation of very few bright carbon stars, and has approximately the right metallicity. It does not produce quantitative agreement since the inferred AGB tip luminosity and progenitor masses are too high.

This model should be thought of as an upper limit to the bulge ZAMS mass. The choice of He/H and O/H are as low as possible and the CSPN mass is as high as possible. This choice of parameters produces the largest possible ZAMS mass since the lower Y is and the higher the ZAMS mass, the larger the resulting CSPN mass.

An advantage of the Wang & Liu fit is since it has well defined trends it is possible to compare the inferred ZAMS N/O to the observed chemical evolution of the Universe. In Table 4 are the typical parameters of less metal-rich and presumably older ZAMS stars are shown. Figure 11 shows the cosmic evolution of N/O as a function of O/H. The positions of both galactic and extragalactic HII regions and some B stars are indicated. For comparison purposes the inferred ZAMS O/H and N/O of the Wang & Liu fits (indicated by the large circles) are also plotted. The inferred position of the GB-PNe on the N/O-O/H plane are comparable to the positions of HII regions and unevolved stars. The chemical evolution of nitrogen suggested by the GB-PNe suggests the chemical evolution of the bulge is consistent with what is seen elsewhere in the Universe. The GB-PNe show an upward slope of N/O as a function of O/H. This is consistent with the upward slope of N/O versus O/H seen in HII regions and stars. This trend is interpreted as indicating the production of secondary nitrogen becoming important (Henry, Edmunds and Köppen 2000). The conclusion is chemical evolution models of the bulge need to include both primary and secondary production of nitrogen.

4.2 Less conservative scenarios

The largest ZAMS mass inferred from the Wang & Liu fit is higher than the MSTOs observed by studies of stars, therefore, models are fit to a series of reasonable assumed parameters which will produce a lower inferred MSTO mass. The sets of global parameters fit are listed in Table 5. These are fits only to the high mass end of the CSPN mass distribution. The primary changes are a decrease in the highest CSPN masses and in some cases an increase in the He/H value. This should give lower ZAMS masses since a lower main sequence mass should give a lower CSPN mass. Higher values of Y on the main sequence lead to larger CSPN masses as well also giving a lower ZAMS mass.

Models are fit to GB-PNe He/H values of 0.130 to 0.140. In Figure 5 the positions of these models are indicated by the large triangles. The triangles seem to be near the top of the He/H distribution as defined in Subsection 3.1. The maximum value He/H is set to is 0.140 because this is the highest value which shows up in all of the GB-PNe sets. The assumed value of O/H for most sets is between 8.85 or 8.90. This seems to agree well with the highest value found in all the GB-PNe sets as indicated in Figure 5. The value of N/O were set to -0.200 to -0.300. Figure 10 shows the position

of these fits which can be seen near the top of all the distributions.

The less conservative models listed in Table 5 are reasonable fits to observations of GB-PNe. The parameters have been chosen to cover a range of possible parameters of the GB-PNe with the highest mass progenitors. They are considered less conservative since the typically assumed CSPN mass is less than $0.62 M_{\odot}$ which will be fit by lower mass ZAMS models. All the models have a supersolar a ZAMS [Fe/H] between +0.2 and +0.3. This agrees with the Bensby et al. 2010 observations of super solar bulge stars. As noted in Subsection 4.1, they find the [Fe/H] of the youngest stars are between +0.15 and +0.5.

The first two models listed in Table 5 are chosen to fit a maximum CSPN mass of $0.60 M_{\odot}$ with two different values of He/H. The inferred progenitor masses of both are $1.6 M_{\odot}$ progenitors. The inferred ages of both stars ≈ 2 Gyr, which is younger than the youngest inferred ages from Bensby et al. (2010, 2011). The model AGB tip magnitudes are. For the first two models in Table 5 the bolometric magnitudes are -4.94 and -4.97 which is close to the observed value (Zoccali et al. 2003).

The third model listed in Table 5 was chosen to fit a maximum CSPN mass of $0.58 M_{\odot}$. This is a CSPN mass as low as is possible which fits the observations. This of course may be too low. The ZAMS mass is $1.4 M_{\odot}$ model has an age around 3.0 Gyr which agrees with the youngest star in the Bensby work. The inferred $M_{AGB-tip} = -4.74$ is in good agreement with the observed value.

None of the first three models listed in Table 5 experience a TDU event although reasonable changes to the parameters in the dredge-up law can give dredge-up events near the tip of the AGB. This observation is consistent with the lack of bulge carbon stars.

4.3 Models with variations in the mass-loss laws

One way to get the models into better numerical agreement the inferred masses of Bensby et al. (2010, 2011) would be to decrease the mass-loss on the TP-AGB. This gives longer TP-AGB lifetimes, allowing the core more time to grow to a higher mass. There are a number of ways of doing this to reduce the mass loss rates, but the way chosen for this study is to increase the mixing length parameter, α . Increasing α makes the star more compact and leads to a decrease in the mass-loss rate. The models where this procedure has been applied are indicated in rows four and seven of Table 5.

In the model in row four the best fitting model is a $1.25 M_{\odot}$ model with slightly higher than solar abundances. This model gives a CSPN mass of $0.59 M_{\odot}$ and indicates the bolometric magnitude of the AGB tip is -4.8 which is in pretty good agreement with the observed value. The pre-TP-AGB lifetime of this model is around 4-5 Gyr. The ZAMS helium abundance of this model is an elevated to ≈ 0.32 .

In the model in row seven the best fitting model is a $1.35 M_{\odot}$ model with super-solar abundances. In this model the relationship between the ZAMS abundances of the α elements and the abundance of iron has been modified. The plateau has been increased to +0.5. This was chosen since when Bensby et al. (2010) plotted [O/Fe] as a function of [Fe/H] the plateau for oxygen (and only oxygen) is at +0.5. What this means is [O/Fe] has a steeper decrease as a func-

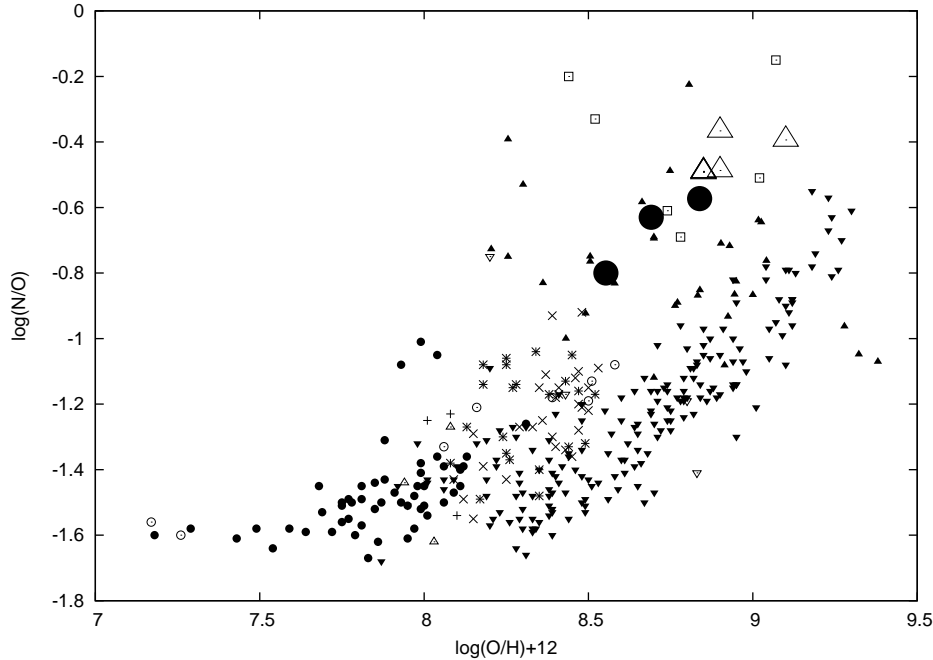


Figure 11. Plotted in this figure is a diagram similar to Figure 1b in Henry, Edmunds and Köppen (2000) which shows the cosmic evolution of N/O as a function of O/H. The figure shows the inferred ZAMS O/H and N/O of both the Wang & Liu fits and the less conservative fits. The large circles and triangles are the Wang & Liu and less conservative fits, respectively. The pluses, Xs, stars, open circles, closed circles, open upright triangles, closed upright triangles are the HII region abundances of Hernández-Martínez et al. (2009), Bresolin et al. (2009), Magrini et al. (2007), Garnett et al. (1999) and references therein, Izotov and Thuan (1999), Kobulnicky and Skillman (1999), Afferbach, Churchwell and Werner (1997), Fich and Silkey (1991), and van Zee et al. (1998), respectively. The open squares are the OB star abundances from Trundle et al. (2002).

Table 5. Parameters to fit for less conservative parameters

CSPN mass	He/H	log(O/H)+12	log(N/O)	M	Y_{ZAMS}	Z_{ZAMS}	[Fe/H]	log(N/O) $_{ZAMS}$	$M_{AGB-tip}$	Notes
0.600	0.130	8.85	-0.300	1.60	0.320	0.0176	0.210	-0.491	-4.94	
0.600	0.140	8.85	-0.300	1.60	0.340	0.0186	0.195	-0.493	-4.97	
0.580	0.130	8.85	-0.300	1.40	0.319	0.0190	0.195	-0.490	-4.74	
0.590	0.130	8.85	-0.303	1.25	0.316	0.0190	0.205	-0.490	-4.80	(1)
0.590	0.130	9.10	-0.220	1.35	0.311	0.0363	0.575	-0.394	-4.91	(2)
0.580	0.135	8.90	-0.200	1.50	0.331	0.0221	0.270	-0.366	-4.74	(3),(4)
0.590	0.135	8.90	-0.300	1.35	0.325	0.0214	0.270	-0.487	-4.86	(1),(3),(4)

The CSPN mass, He/H, log(O/H)+12, and log(N/O) are the values of the PN parameters being fit. M , Y_{ZAMS} , Z_{ZAMS} , [Fe/H] and log(N/O) $_{ZAMS}$ are the model ZAMS parameters of the best fitting model. $M_{AGB-tip}$ is inferred bolometric magnitude of the AGB-tip

(1) This model has its mixing length parameter increased to 2.2 from 1.8 which decreases TP-AGB mass-loss rate.

(2) This is a model fit to a higher O/H value then is indicated by the PNe oxygen abundances.

(3) In these models the pre-AGB mass loss one half of that given by the formulas in Subsection 2.2.

(4) In these models the relationship between the abundances of the α elements and iron was modified. The value of $[\alpha/Fe]$ plateau was set to +0.5. This leads to a steeper decline in [O/Fe] as a function of [Fe/H].

tion of [Fe/H] for [Fe/H]>-1. This means to get the same O/H a higher metallicity is required. This model is probably the best numerical match to the Bensby et al. observations since the implied [Fe/H] of +0.27 and the inferred highest mass progenitor matches their highest mass closely.

loss was reduced to one half the value as determined by the procedure outlined in Subsection 2.2. The result is not significantly different then if the pre-AGB mass loss were calculated normally.

In the sixth model listed in Table 5 the pre-AGB mass

4.4 A model which fits a higher oxygen abundance

As noted in Section 3 there is a possibility the oxygen abundance might be higher than is indicated by the PN abundances. The PN parameters fit and the ZAMS parameters used to fit it are indicated in Table 5. With an nearly double oxygen abundance this has a much higher value of Z , which is closer to the Bensby results than the other results. The mass of the fit is $1.35 M_{\odot}$, which is also close to the Bensby result. The ZAMS value of Y is ≈ 0.31 .

4.5 Summary of models

All of the models above are reasonable fits to the GB-PNe trends. They all produce CSPN masses and AGB tip luminosities comparable to the observations. None of them would produce luminous carbon stars except via blue stragglers (not modeled in this paper). All of the implied ZAMS abundances are comparable to what is seen elsewhere. All of the models consistently require an ZAMS value of Y between 0.31 and 0.34. The conclusion is the highest mass bulge ZAMS stars should have Y in this range. The inferred ZAMS N/O ratios are greater than the solar N/O. In all models the ZAMS C/O is less than 1. This agrees with the lack of bright carbon stars in the bulge. More observations of bulge C/O are needed to quantitatively constrain carbon.

5 DISCUSSION

From these models it is concluded it is possible, with reasonable choices of input parameters, to get a qualitative agreement with the observations. All the different assumed scenarios result in essentially no luminous carbon stars which matches the observations. The ZAMS masses and ages needed to reproduce the CSPN masses are reasonably close to the inferred ZAMS masses of Bensby et al. (2010, 2011). The model AGB tip luminosities are in good agreement with the measured luminosities of Zoccali et al. (2003).

If these models are correct they indicate that the element helium had a different chemical evolution in the bulge compared to its evolution in the disc. With the exception of the high oxygen abundance model, for the models to reproduce these GB-PNe the ZAMS values of Y are consistently ~ 0.32 . The Z values needed to fit the most massive models range from ~ 0.019 to 0.22. If a primordial values of the helium abundance, Y_0 , between 0.24-0.25 are assumed this means for the bulge $\frac{dY}{dZ} \approx 4$. This is significantly higher than the typical values of 1.4-1.8 which are typically quoted. Using a typical values of $\frac{dY}{dZ}$ and Y_0 a star with a $Z = 0.019$ should have values of Y between 0.26 and 0.29 indicating. The model with a higher oxygen abundance also required an elevated Y of 0.31 to produce the highest He/H values of GB-PNe.

In all of the models of the highest mass progenitors, both the Wang & Liu and the less conservative models, the ZAMS ratio of N/O had to be increased above the solar ratio to match the observed GB-PNe N/O. To match the typical nitrogen abundances it was necessary to enhance the nitrogen abundance. The typical ZAMS N/O ratio was between 1/4 and 1/3 which is higher than the ratio for the Sun

($\sim 1/9$). This is approximately a factor of 3 enhancement over the solar ratio.

All of this suggests that the younger bulge stars have been enhanced by stars ejecting the products of the CNO cycle. As shown in figure 11 the ZAMS N/O for the less conservative and the Wang & Liu scenarios is consistent with bulge chemical evolution scenarios where nitrogen is produced as both a primary and a secondary element. As a secondary element the nitrogen yield is dependent on metallicity. It is not surprising then that the starting N/O of these stars is higher than solar.

Where is the extra helium synthesized? One possibility for the site of this production is intermediate-mass stars. Bensby et al. 2010, 2011 found a bimodal distribution in [Fe/H] and the age of the microlensed stars. One of the peaks contains stars with subsolar [Fe/H] and typical ages of 10-12 Gyrs. The other peak contained stars with [Fe/H] typically between 0 and +0.5 and younger ages ranging from 3-7 Gyrs in age. There appears to be a gap in the distribution of [Fe/H] indicating star formation stopped for a time. The older population would have formed quickly. Because of this quick formation would have incorporated the products of supernovae of type II and not that of type I supernova and intermediate-mass stars. The high-mass and intermediate-mass members of this older population would then have polluted the interstellar medium (ISM) with helium-rich material. If the existing ISM were very low mass this could potentially lead to an over-enrichment of helium.

5.1 Can the observations be reproduced with intermediate-mass stars?

Marigo et al. (2003) compared synthetic TP-AGB models to the abundances of PNe. For Marigo et al. 2003 to produce the high values of He/H near 0.13 stars of mass $\gtrsim 3.5 M_{\odot}$ were required. A star of this mass would, according to the AGB tracks in Bertelli et al. (2009), produce a CSPN of $0.72 M_{\odot}$ and an AGB tip magnitude of -5.7. This does not match the observations, and unless the galactic centre is significantly farther away than believed, this scenario is excluded. Also if this intermediate-mass star scenario is correct, there would be stars in the bulge of the right mass to produce bright carbon stars, this is not observed in the bulge. All of this together suggests that stars massive ($> 2.0 M_{\odot}$) enough to produce the enhanced helium abundance do not exist in large numbers in the bulge. Therefore, the intermediate-mass star scenario is ruled out.

5.2 Can these observations be reproduced by a very low-mass star?

To test the question if a star with an age of ~ 10 Gyr could reproduce the observations a lower mass model has been run. This is the approximate age found by Zoccali et al. (2003) for the galactic bulge. For $Y \approx 0.30$ this would require a star with main sequence mass $\sim 1 M_{\odot}$. The model parameters were adjusted to fit He/H=0.130 and $\log(O/H) + 12 = 8.85$. A reasonable model is found with $M_{\text{ZAMS}}=1.05 M_{\odot}$, [Fe/H]=0.19, $Y = 0.314$ and $Z = 0.0199$. However, the CSPN mass of this is only $0.56 M_{\odot}$. This is lower than the observed maximum mass CSPN in the Galactic bulge.

6 CONCLUSIONS AND RECOMENDATIONS FOR FUTURE WORK

This study has shown

(i) Reasonable TP-AGB models with low-mass progenitors ($1.2-1.8 M_{\odot}$) and with enhanced Y and N/O on the ZAMS can at least qualitatively match the observations of the GB-PNe. This match includes the observed values in GB-PNe of He/H , O/H , N/O and the CSPN mass. These models also qualitatively match the bulge's AGB tip luminosity and are consistent with little or no formation of bright carbon stars.

(ii) The inferred N/O values for the progenitor ZAMS stars are consistent with what is known about the cosmic evolution of nitrogen. The implication is the secondary production of nitrogen is important in the chemical evolution of the Galactic bulge.

(iii) Very low-mass ($M \approx 1 M_{\odot}$) and intermediate-mass ($M \gtrsim 3.5 M_{\odot}$) are not able to match the observed CSPN masses. Unless the CSPN masses are very different from what is observed the bulge, the very low- and intermediate-mass stars would produce CSPN masses that are either too low or too high, respectively. The intermediate-mass star scenario would produce very bright carbon stars which are not observed.

(iv) The youngest stars in the bulge are probably between 2 and 5 Gyrs in age and have a slightly higher metallicity than the Sun ($Z \approx 0.019$ to 0.022) and a significantly higher value of Y (≈ 0.32 to 0.34) than a disc star of the same metallicity. This is in rough agreement with the results of Bensby et al. (2010, 2011) for bulge main sequence and sub-giant branch stars.

(v) These models indicate the last galactic bulge stars formed between 2 and 4 Gyrs of age. This should be thought of as an intermediate age population.

(vi) The implied C/O of most of the GB-PNe is less than 1. This requires a ZAMS $C/O < 1$.

Some recommendations for future work include: Better values of the CSPN mass need to be determined. A big limitation of this study is the poor knowledge of the CSPN masses so any improvements would lead to better limits on the range of possible models. Future microlensing studies of bulge stars should include carbon and nitrogen abundances if possible. This paper predicts the ratio of N/O of super-solar stars should be enhanced relative to the solar values.

ACKNOWLEDGMENTS

I would like to acknowledge the support of a Alfred State College Faculty Scholarship Grant which supported this work during the Spring 2012 semester. I would also like to thank R.B.C. Henry for reading an earlier manuscript and making comments which have improved this paper. I would like to acknowledge the contribution of the papers referee, D.M. Nataf, whose comments considerably improved the paper.

REFERENCES

- Afflerbach A., Churchwell E., Werner M.W., 1997, ApJ, 478, 190
- Alexander D.R. and Ferguson J.W., 1994, ApJ, 437, 879
- Asplund M., Grevesse N., Sauval A.J., 2005, in ASP Conf. Ser. 336, Cosmic Abundances as Records of Stellar Evolution and Nucleosynthesis, ed. F.N. Bash & T.G. Barnes
- Azzopardi M., Lequeux J., Rebeirot E., 1988, A&A, 202, L27
- Bensby, T., Feltzing, S., Johnson, J.A. et al., 2010, A&A, 512, A41
- Bensby, T. et al., 2011, A&A, 533, A134
- Bertelli G., Girardi L., Marigo P., and Nasi E., 2008, A&A, 484, 815
- Bertelli G., Nasi E., Girardi L. and Marigo P., 2009, A&A, 508,355
- Blöcker T., 1995, A&A, 299, 755
- Boothroyd A.I., Sackmann I.-J., 1999, ApJ, 510, 232
- Bresolin F., Gieren W., Kudritzki R.-P., Pietrzyński, Urbaneja M.A., Carraro G., 2009, ApJ, 700, 309
- Brown T.M. et al., 2010, ApJ, 725, L19
- Buell J.F., 2012, MNRAS, 419, 2867
- Buell J.F., Henry R.B.C., Baron E., Kwitter K.B., 1997, ApJ, 483, 837
- Buell J.F., 1997, PhD thesis, Univ. Oklahoma
- Catalán S., Isern J., García-Berro E., Ribas I., 2008, MNRAS, 387, 1693
- Chiappini C., Górny S.K., Stasińska G., Barbay B., 2009, A&A, 494, 591
- Clarkson W.I. et al., 2011, ApJ, 735, 37
- Cuisinier, F., Maciel, W.J., Köppen, J., Acker, A., & Stenholm, B. 2000, A&A, 353, 543
- Dominguez I., Straniero O., Tornambe A., Isern J., 1996, ApJ, 472, 783
- Dominguez I., Chieffi A., Limongi M., Straniero O., 1999, ApJ, 524, 226
- Escudero A.V., Costa R.D.D., Maciel W.J., 2004, A&A, 414, 211
- Exeter K.M., Barlow M.J., Walton N.A., 2004, MNRAS, 349, 1291
- Fich M., Silkey M., 1991, ApJ, 366, 107
- Garnett D.R., Shields G.A., Peimbert M., Torres-Peimbert S., Skillman E.D., Dufour R.J., Terlevich E., Terlevich R.J., 1999, ApJ, 513, 168
- Gavilan M., Buell J.F., Molla, M., 2005, A&A, 432, 861
- Ghez, A.M. et al., 2008, ApJ, 689, 1044
- Gratton R.G., Carretta E., Bragaglia A. 2011, preprint (astro-pn/1201.6526)
- Gratton R.G., Carretta E., Bragaglia A., Lucatello S. & D'Orazi V., 2010, A&A, 517, 81
- Groenewegen M.A.T. and de Jong T., 1993, A&A, 267, 410
- Gutenkunst S., Bernard-Salas J., Pottasch S.R., Sloan G.C., Houck J.R., 2008, ApJ, 680, 1260
- Guzman-Ramirez L., Zijlstra A.A., Ní Chuimín R., Gesicki K., Lagadec E., Millar T.J., Woods P.M., 2011, MNRAS, 414, 1667
- Henry R.B.C., Edmunds M.G., Köppen J., 2000, ApJ, 541, 660
- Hernández-Martínez L., Peña M., Carigi L., García-Rojas J., 2009, A&A, 505, 1027
- Hultsch P.J.N., Puls J., Méndez R.H., Pauldrach A.W.A.,

- Kudritzki R.-P., Hoffmann T.L., McCarthy J.K., 2007, *A&A*, 467, 1253
- Iglesias C.A. and Rogers F.J., 1996, *ApJ*, 464, 943
- Izotov Y.I., Thuan T.X., 1999, *ApJ*, 511, 639
- Izotov Y.I., Thuan T.X., 2010, *ApJ*, 710, L67
- Kalirai J.S., Richer H.B., Reitzel D., Hansen B.M.S., Rich R.M., Fahlman G.G., Gibson B.K., von Hippel T., 2005, *ApJ*, 618, L123
- Kobulnicky H.A., Skillman E.D., 1999, *ApJ*, 467, 601
- Kuijken K., Rich R.M., 2002, *AJ*, 124, 2054
-] Liu X.-W., 2006, in Barlow M.J., Menedez R.H. eds, *Proc. IAU Symp. 234, Planetary Nebulae in Our Galaxy and Beyond*. Astron. Soc. Pac., San Francisco, p. 219
- Liu X.-W., Luo S.-G., Barlow M.J., Danzinger I.J., Storey P.J. 2001, *MNRAS*, 327, 141
- Magrini L., Vilchez J.M., Mampaso A., Corradi R.L.M., Leisy P., 2007, *A&A*, 470, 865
- Marigo P., 2001, *A&A*, 370, 194
- Marigo P., Bernard-Salas J., Pottasch S.R., Tielens A.G.G.M., Wesselius P.R., 2003, *A&A*, 409, 619
- Marigo P., Girardi L., Bressan A., 1999, *A&A*, 344, 123
- Meng X., Chen X., Han Z., 2008, *A&A*, 487, 625
- Miglio A. et al., 2012, *MNRAS*, 419, 2077
- Nataf D.M., Gould A.P., 2012, *ApJ*, 751, L39
- Nataf D.M., Udalski A., Gould A., Pinsonneault M.H., 2011, *ApJ*, 730, 118
- Perea-Calderón J.V., García-Hernández D.A., García-Lario P., Szczerba R., Bobrowsky M., 2009, *A&A*, 495, L5
- Piotto G., 2009, in *Proceedings IAU Symposium 258*, 233, eds. E.E. Mamajek, D.R. Soderblom, R.F.G. Wyse
- Ratag M.A., 1991, Ph.D thesis, Groningen University
- Ratag M.A., Pottasch S.R., Dennefeld M., Menzies J.W., 1992, *A&A*, 255, 255
- Ratag M.A., Pottasch S.R., Dennefeld M. & Menzies J., 1997, *A&AS*, 126, 297
- Reimers D., 1975, *Mem. Soc. R. Sci Liège*, 8, 369
- Renzini, A. 1979, in *Stars and Systems*, ed. B.E. Westerlund (Dordrecht: Reidel), p. 155
- Renzini A., Voli M., 1981, *A&A*, 94, 175
- Schröder K.P., Cuntz M., 2005, *ApJ*, 630, L73
- Schönberner D., 1981, *A&A*, 103, 119
- Schönberner D., 1983, *ApJ*, 272, 708
- Simón-Díaz S., Nieva M.F., Przybilla N., Stasińska G., 2011, *BSRSL*, 80, 255
- Stanghellini L., García-Hernández D.A., García-Lario P., Davies, J.E., Shaw R.A., Villaver E., Manchado A., Perea-Calderón J.V., 2012, preprint (astro-ph/1205.3829)
- Stasińska G., Tylenda R., Acker A., Stenholm B., 1991, *A&A*, 247, 173
- Trundle C., Dufton P.L., Lennon D.J., Smartt S.J., Urbaneja M.A., 2002, *A&A*, 395, 519
- Tylenda R., Stasińska G., Acker A., Stenholm B., 1991, *A&A*, 246, 221
- Uttenthaler S., Hron J., Lebzelter T., Busso M., Schultheis M., Käufel H.U., 2007, *A&A*, 463, 251
- van Zee L., Salzer J.J., Haynes M.P., O'Donoghue A.A., Balnock T.J., 1998, *AJ*, 116, 2805
- Vassiliadis V.W., Wood P.R., 1993, *ApJ*, 413, 641
- Vassiliadis V.W. & Wood P.R., 1994, *ApJS*, 92, 125
- van Saders J.L., Pinsonneault M.H., 2012, *ApJ*, 746, 16
- Wang W., Liu X.-W. 2007, *MNRAS*, 381, 699
- Wagenhuber J., Groenewegen M.A.T., 1998, *A&A*, 340, 183
- Weidemann V., 1977, *A&A*, 59, 418
- Weidemann V., 2000, *A&A*, 363, 647
- Zoccali, M. et al., 2003, *A&A*, 399, 931